DISCLAIMER

This report was prepared as an account of work sponsored by an agency of the United States Government. Neither the United States Government nor any agency thereof, nor any of their employees, makes any warranty, express or implied, or assumes any legal liability or responsibility for the accuracy, completeness, or usefulness of any information, apparatus, product, or process disclosed, or represents that its use would not infringe privately owned rights. Reference herein to any specific commercial product, process, or service by trade name, trademark, manufacturer, or otherwise does not necessarily constitute or imply its endorsement, recommendation, or favoring by the United States Government or any agency thereof. The views and opinions of authors expressed herein do not necessarily state or reflect those of the United States Government or any agency thereof. Reference herein to any social initiative (including but not limited to Diversity, Equity, and Inclusion (DEI); Community Benefits Plans (CBP); Justice 40; etc.) is made by the Author independent of any current requirement by the United States Government and does not constitute or imply endorsement, recommendation, or support by the United States Government or any agency thereof.

SANDIA REPORT
SAND2025-07335
Printed June 2025

Sandia National Laboratories

Notes on Bayliss Taper for Monopulse Radar

Armin W. Doerry and Douglas L. Bickel

Prepared by
Sandia National Laboratories
Albuquerque, New Mexico
87185 and Livermore,
California 94550

Issued by Sandia National Laboratories, operated for the United States Department of Energy by National Technology & Engineering Solutions of Sandia, LLC.

Available to DOE and DOE contractors from
U.S. Department of Energy
Office of Scientific and Technical Information
P.O. Box 62
Oak Ridge, TN 37831

Telephone: (865) 576-8401
Facsimile: (865) 576-5728
E-Mail: reports@osti.gov
Online ordering: http://www.osti.gov/scitech

Available to the public from
U.S. Department of Commerce
National Technical Information Service
5301 Shawnee Rd
Alexandria, VA 22312

Telephone: (800) 553-6847
Facsimile: (703) 605-6900
E-Mail: orders@ntis.gov
Online order: https://classic.ntis.gov/help/order-methods/

Notes on Bayliss Taper for Monopulse Radar

Armin W. Doerry, Douglas L. Bickel

Abstract

A radar system's antenna characteristics are fundamental to its performance. A principal defining feature of an antenna's performance are its often problematic sidelobes. Often in monopulse antenna topologies, the emphasis has been on the sum channel sidelobes at the expense of difference channel sidelobes. Edward Bayliss published a paper detailing a design procedure for managing the difference channel sidelobes. The resulting aperture taper now is identified by his name. This report analyzes his taper derivation, and resulting performance attributes, after which some implementation comments are rendered.

Acknowledgements

The authors wish to thank Sam Davis for his detailed review and helpful suggestions for this report.

This report is the result of a Cooperative Research and Development Agreement (CRADA) between Sandia National Laboratories and General Atomics Aeronautical Systems, Inc. – CRADA No. SC08/01749.

GA-ASI, an affiliate of privately-held General Atomics, is a leading manufacturer of unmanned aircraft systems (UAS), tactical reconnaissance radars, and surveillance systems, including the Predator UAS series and Lynx Multi-Mode radar systems.

Sandia National Laboratories is a multimission laboratory managed and operated by National Technology & Engineering Solutions of Sandia LLC, a wholly owned subsidiary of Honeywell International Inc. for the U.S. Department of Energy's National Nuclear Security Administration under contract DE-NA0003525.

Contents

List of Figures

List of Tables

Acronyms and Definitions

AESA	Active Electronically Steered/Scanned Array
DOA	Direction of Arrival
DSP	Digital Signal Processing
GMTI	Ground Moving Target Indicator [radar]
IPR	Impulse Response
ISR	Intelligence, Surveillance, and Reconnaissance
PRF	Pulse Repetition Frequency
RX	Receive, Receiver
SAR	Synthetic Aperture Radar
SNR	Signal-to-Noise Ratio
TX	Transmit, Transmitter

Foreword

This report details the results of an academic study. It does not intend to exemplify any modes, methodologies, or techniques employed by any specific system, operational or experimental. Any resemblance to such is accidental and inadvertent.

Classification

The specific mathematics and algorithms presented herein do not bear any release restrictions or distribution limitations.

This report formalizes preexisting informal notes and other documentation on the subject matter herein.

This report has been approved for distribution without limitations.

Author Contact Information

Armin Doerry awdoerr@sandia.gov 505-845-8165 www.doerry.us

1 Introduction and Background

Perhaps no single component in a typical radar system has a greater impact on overall performance than the antenna. It is a transducer between the circuitry of radar hardware and propagating electromagnetic fields, for both generating those Transmitted (TX) fields, and sensing the Received (RX) fields. By virtue of its beamwidth, the antenna serves as a spatial filter, with gain and sensitivity in some directions at the expense of others.

In sensing RX fields, we generally desire accurate and precise knowledge of the Direction of Arrival (DOA) for the RX energy. The directivity or gain of a RX antenna pattern is usually designed to peak in a specific direction, but also offers some angular width to a lobe of sensitivity around the peak. Absent any additional information, a single static antenna beam when pointed in a single direction, can only presume to locate the DOA of a RX signal to 'within the mainlobe' of the antenna. To refine the DOA accuracy and precision to something finer than merely in the antenna's mainlobe requires additional information. This additional information comes in the form of additional antenna beams with some diversity in either their mainlobe direction, or with some diversity in their physical location, or sometimes perhaps both.

In this report, we shall examine a topology with spatially separated RX antennas, identifying this architecture as a "Phase Monopulse" topology.[†] In fact, we will constrain ourselves in this report to analyzing a 1-Dimensional antenna aperture where two antenna phase centers are created by dividing the overall RX antenna aperture into left-half and right-half subapertures. We thereby create an interferometer between left-half and right-half subapertures.

Often, the signals from these halves might be coherently added in phase to create a "sum" signal, or reference signal, which exhibits a "sum pattern" over DOA angles for directivity.[‡] Otherwise, or in addition, the signals from these halves might have one subtracted from the other to create a "difference" signal, which exhibits a "difference pattern" over DOA angles for directivity.[§] This subtraction may be implemented by suitable phase shifting and adding.

An antenna's far-field directivity pattern is determined by the weighting applied to the overall antenna aperture. This is sometimes called an aperture illumination function. The aperture weighting and directivity pattern constitute a Fourier Transform pair. Creating a directivity pattern from a taper function is often called "beamforming." The tapering is usually intended to control characteristics of the directivity pattern such as mainlobe shape and sidelobe levels. Antenna sidelobes for RX antennas are problematic in allowing energy from undesired DOA angles to enter the signal stream. The aperture weighting to control this is generally real-valued,

---

[†] Multiple antenna beams with diversity in their mainlobe direction would constitute an "Amplitude Monopulse" topology.

[‡] We emphasize that this reference signal is generated from over the entire aperture, not just a segment from it.

[§] We note that in a typical antenna beam mainlobe, there is a one-to-one correspondence between specific DOA within the mainloabe, and the derivative of the mainlobe directivity function with DOA. So, if we can measure the angular derivative of the directivity response, then we should be able to locate the specific DOA even within the mainlobe response of the received energy. We further note that deriviatives are estimated from difference responses. This is the essence of classical monopulse processing.

with symmetry. The sum pattern results from even symmetry of the taper, and the difference pattern results from an odd symmetry of the taper. The magnitude function of the tapers need not be the same, but nevertheless often are. In cases where the magnitudes are the same, the taper for the difference pattern results from negating the weighting (applying a π phase shift) for either the left half of the aperture or the right half of the aperture, thereby forcing the desired odd symmetry.[**] This substantially simplifies the overall beamforming process.

We note that from basic Fourier Transform properties, for a sum taper that is real and even, then the sum pattern is also real and even. However, if the difference taper is real and odd, then the difference pattern is imaginary and odd.

In the usual case where the sum and difference tapers have the same magnitude, then the sum taper over the whole aperture is typically designed first to optimize the sum pattern for mainlobe response and sidelobe control. The difference taper is then simply created by negating the weighting for half the aperture. This is accomplished with a monopulse network.[††] This results in the difference pattern exhibiting fairly large sidelobes, even when the sum pattern does not.

Edward Bayliss published a paper in 1968 in the Bell System Technical Journal that took a somewhat different approach.[1] In it he notes

> "The flexibility of modern monopulse radar antenna systems makes possible the independent optimization of sum and difference patterns."

He further stipulates in his paper

> "The objective of this investigation was to develop a difference pattern which possesses characteristics that are compatible with those of the Taylor [taper] sum pattern. Specifically, the goal was to obtain the maximum angle sensitivity commensurate with a given sidelobe level. Low sidelobes are desirable in both sum and difference patterns for the suppression of near-target clutter, ground clutter, and jammers. Requiring large angle sensitivity and low sidelobes for the difference pattern is analogous to requiring a narrow beamwidth and low sidelobes in the case of the sum beam. The pattern that meets these requirements must be produced by a reasonably well behaved aperture illumination."

In other words, Bayliss sought to optimize the performance of the difference pattern, the sum pattern notwithstanding. He assumed that the sum pattern could be formed independent of the difference pattern. Although fully independent sum and difference patterns complicate the beamforming process, Bayliss nevertheless judged this to be "feasible."

[**] We note that we are here referring to the RX antenna. The TX antenna is not necessarily constrained to the same aperture weighting as the RX sum taper. It may or may not be.

[††] The monopulse network is also often called a "monopulse comparator, "magic T," "arithmetic network," "monopulse hybrid," or any of a variety of other names.

Our interest in this report is for array antennas, specifically programmable Active Electronically Steered Array (AESA) antennas, and the elemental weightings necessary to define a directivity pattern for optimum performance.

As background for this report, and to somewhat help guide us in the subsequent analysis, we offer several reference publications. With apologies to the larger radar community, we acknowledge that this list is not at all complete.

> An iconic text that discusses monopulse principles generally is by Sherman and Barton.[2]
>
> The equivalence of Amplitude and Phase Monopulse performance was discussed in an earlier report.[3]
>
> Window taper functions in general were discussed in another earlier report.[4]
>
> The effects of tapers on array antenna performance were discussed in yet another earlier report.[5]

Several publications discuss details of the Bayliss taper specifically.

> A text that discusses array antennas in general, with a section on Bayliss tapers, is offered by Mailloux.[6]
>
> Similarly, a text by Elliott also discusses details of the Bayliss taper development.[7]
>
> A report by Shelton gives design equations for both Taylor and Bayliss tapers.[8]
>
> A report that presents the theory related to the design of Taylor and Bayliss tapers is given in a paper by Zinka and Kim.[9]

Aspects of the Baylis taper are also given in several other publications.[10,11]

Other publications yet discuss the role of a Bayliss taper in monopulse antenna performance generally.[12,13,14]

Elliot also discusses an extended design technique "which will yield difference patterns with arbitrary sidelobe topographies."[7,15]

Indeed, other techniques and algorithms exist to optimize difference patters, including those that use Zolotarev polynomials.[16,17,18,19,20,21,22]

We note that tapers have also been investigated that impose dependencies between sum and difference tapers in an attempt to optimize both somewhat without two entirely independent beamformers, often with subarray structures.[23,24]

While Bayliss' technique addresses phase monopulse tapers, we acknowledge that amplitude monopulse antenna optimization with respect to sidelobes has also been studied.[25,26,27,28]

“You only have to do a very few things right in your life so long as you don't do too many things wrong.”
― Warren Buffett

2 Derivation of the Bayliss Taper

The pedigree of the Bayliss taper development derives from the development of the Taylor window taper function,[29,30] itself an approximation to the Dolph taper, also called the Dolph-Chebyshev taper.[31] Bayliss himself stated that

> "This paper solves the problem of generating difference patterns by using a technique that parallels Taylor's approach to the sum pattern design."

While Bayliss focused his attention on a circular aperture, he did also address a line source in the appendix to his paper. In this report we will concern ourselves more with the line source development, as this is more readily extensible to rectangular apertures which are more relevant to our work.

What follows in this section is a review of the development by Baylis for a line source. We will use his nomenclature for parameters for our review. We will also provide some commentary to the development, and correct some apparent typographical errors.

Some Preliminary Notes

We first define a line source with finite length

$2a$ = length of line source. (1)

Bayliss normalizes the length with respect to π/a such that the position along the line source is constrained to

$$-\pi \le x \le \pi\,. \tag{2}$$

The aperture illumination function is

$g(x)$ = aperture illumination function. (3)

Note that

$$g(x) = 0 \text{ for } |x| > \pi\,. \tag{4}$$

The far-field antenna pattern generated by this line source is given as the Fourier Transform of the aperture illumination function, which Bayliss identifies as

$$F(u) = \int_{-\infty}^{\infty} g(x) e^{jux} dx = \int_{-\pi}^{\pi} g(x) e^{jux} dx\,, \tag{5}$$

where

$u = (2a/\lambda)\sin\theta$,
λ = signal wavelength, and
θ = angle measure from the normal to the line source. (6)

The Goal

Since we are dealing with a difference pattern, Bayliss chooses to model it as a finite sum of sine functions, namely

$$g(x)=\begin{cases}\sum_{l=0}^{N-1} B_l \sin(\mu_l x) & -\pi \le x \le \pi \\ 0 & else\end{cases}, \tag{7}$$

where

B_l = coefficients that we will need to find,
N = number of terms to sum, and
μ_l = frequency term. (8)

Note that l is an integer. Now for some comments.

- We stipulate that the coefficients B_l are allowed to be complex (i.e., not limited to real values).
- The number of terms N is analogous to the Taylor window parameter often identified as nbar or $\bar{n}$. It identifies approximately the point in the taper function Impulse Response (IPR) where otherwise equal-level sidelobes begin to increasingly diminish with distance from peak value.
- Bayliss identifies that a nonzero boundary value is required for the truncated series. Consequently, we limit

  $$\mu_l = l + 1/2, \tag{9}$$

  The Bayliss paper appears to contain a typographical error regarding this.

Performing a Fourier Transform on Eq. (7) yields

$$F(u) = 2j\sum_{l=0}^{N-1} B_l \frac{(-1)^l u\cos(\pi u)}{(l+1/2)^2 - u^2} \tag{10}$$

This is the IPR of the aperture illumination function identified in Eq. (7) above. It describes the far-field antenna pattern resulting from the taper. This is also Eq. 42 in the Bayliss paper, although the Bayliss paper again exhibits a minor typographical error in the argument of the cosine terms.

Our goal is to identify the coefficients B_l. This entails equating Eq. (10) to an ideal "asymptotic difference pattern."

The Asymptotic Model Difference Pattern

Bayliss begins with the ideal sum pattern used by Taylor as of the form

$$F_{\Sigma}(u) = \cos\left(\pi\sqrt{u^2 - A^2}\right), \tag{11}$$

where

A = constant that determines maximum allowable sidelobe level. (12)

This ideal sum pattern has equal sidelobes for an infinite extent. The derivative of Eq. (11) yields a difference pattern which we calculate as

$$F_{\Delta}(u) = \pi\left(u^2 - A^2\right)^{-1/2} u \sin\left(\pi\left(u^2 - A^2\right)^{+1/2}\right). \tag{13}$$

This is Eq. (12) in Bayliss' paper. Bayliss notes that "The first few sidelobes of this function are not of equal height." He also states that "However, it is possible to modify the first few sidelobes of the above function so that they are equal to the asymptotic sidelobe level." The zeros of Eq. (13) are identified as

$$z_n = \begin{cases} 0 & n = 0 \\ \pm\left(n^2 + A^2\right)^{+1/2} & n = 1, 2, 3, \cdots \end{cases}. \tag{14}$$

By moving the first several zeros, Bayliss creates a "Model" difference function as

$$F_M(u) = F_{\Delta}(u) \prod_{n=1}^{T} \frac{\xi_n^2 - u^2}{z_n^2 - u^2} \quad = \text{Model difference function,} \tag{15}$$

where

ξ_n = the position to which z_n is moved, and
T = the number of zeros on either side of the mainlobe that are moved. (16)

Now for some comments.

- Bayliss identifies that "Very good results were obtained by moving only the first four zeros on either side of the origin." This implies that good results are given with $T = 4$.
- Specific values for A and ξ_n will depend on the desired sidelobe levels in the final IPR of the difference pattern. Bayliss fit a fourth-order polynomial to these parameters as a function of sidelobe level which gives reasonably good results over the span of sidelobe levels from −15 dB to −60 dB relative to the difference pattern peak value. Polynomial coefficients are given in Table 1, with plots given in Figure 1.
- Bayliss also identifies the location of the difference pattern peaks at $u = \pm p_0$.

Table 1. Parameter Polynomial Coefficients. This table reproduces the data in Fig. 4 of the Bayliss paper.

Parameter	Polynomial Coefficients				
	C_0	C_1	C_2	C_3	C_4
A	0.30387530	-0.05042922	-0.00027989	-0.00000343	-0.00000002
ξ_1	0.98583020	-0.03338850	0.00014064	0.00000190	0.00000001
ξ_2	2.00337487	-0.01141548	0.00041590	0.00000373	0.00000001
ξ_3	3.00636321	-0.00683394	0.00029281	0.00000161	0.00000000
ξ_4	4.00518423	-0.00501795	0.00021735	0.00000088	0.00000000
p_0	0.47972120	-0.01456692	-0.00018739	-0.00000218	-0.00000001

The parameters are calculated as

$$\text{Parameter} = \sum_{k=0}^{4} \left(C_k S_{dB}^k \right) \quad , \tag{17}$$

where

S_{dB} = sidelobe level with respect to difference pattern peak in dB. (18)

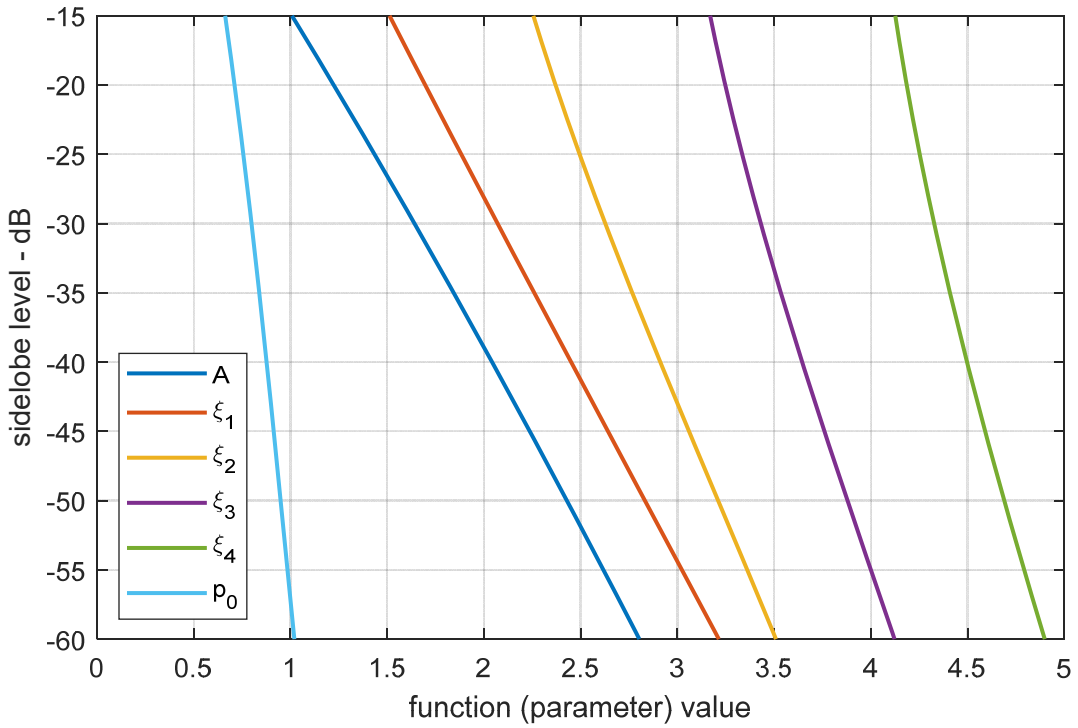

Figure 1. Parameter values as a function of sidelobe level using polynomial approximations. This table reproduces the plots in Fig. 4 of the Bayliss paper.

As Bayliss observes, “The use of fitted polynomials inevitably leads to errors in the results. The effect of these errors is more pronounced in the low sidelobe pattern.” If better fidelity is required, then Bayliss advises “to use the calculated zeros directly and avoid use of the polynomials.” Nevertheless, over the sidelobe levels indicated, the polynomials work quite well.

We observe that $F_M(u)$ is completely described by its zeros, which are located at

$$Z_n = \begin{cases} 0 & n = 0 \\ \pm\xi_n & n = 1,\cdots,T \\ \pm\sqrt{A^2 + n^2} & n = T+1,\cdots \end{cases}, \tag{19}$$

Note that for large $|n|$ the zeros approach $\pm n$ asymptotically. However, the equal sidelobe levels for all sidelobes in $F_M(u)$ is not realizable due to finite energy constraints. This is remedied by moving all sidelobe zeros for $|n| \geq N$ to μ_n. This in turn causes another problem of a problematic transition region for sidelobe behavior in the $|n| = N$ region. This is then compensated by “dilating” the zero positions for $|n| < N$ in the manner of scaling their location to the new position

$$\sigma Z_n = \text{new zero positions for } |n| < N, \tag{20}$$

where

$$\sigma = \frac{\mu_N}{Z_N} = \frac{N + 1/2}{Z_N} = \text{dilation factor.} \tag{21}$$

We may now describe the asymptotic model for the difference function as the canonical product

$$F_a(u) = Cu \prod_{n=1}^{N-1} \left(1 - \left(\frac{u}{\sigma Z_n}\right)^2\right) \prod_{l=N}^{\infty} \left(1 - \left(\frac{u}{\mu_l}\right)^2\right), \tag{22}$$

where

$$C = \text{a constant.} \tag{23}$$

Bayliss states “The constant C is evaluated so that the peak of the asymptotic difference pattern is unity.” The implication is that it is real-valued. More on this later.

Noting Eq. (9), we identify the product expansion

$$\cos \pi u = \prod_{l=0}^{\infty} \left(1 - \left(\frac{u}{\mu_l} \right)^2 \right) . \tag{24}$$

This allows the asymptotic model for the difference function to be expressed as

$$F_a(u) = Cu \cos(\pi u) \left\{ \frac{\prod_{n=1}^{N-1} \left(1 - \left(\frac{u}{\sigma Z_n} \right)^2 \right)}{\prod_{l=0}^{N-1} \left(1 - \left(\frac{u}{\mu_l} \right)^2 \right)} \right\} . \tag{25}$$

This function has poles at $u = \mu_l = l + 1/2$. At these pole positions, $\cos(\pi u) = 0$. This is zero for every integer index *l*. So, at these pole positions, we have zeros in both numerator and denominator. To deal with this, we may rewrite this as

$$F_a(u) = Cu \left(\prod_{n=1}^{N-1} \left(1 - \left(\frac{u}{\sigma Z_n} \right)^2 \right) \right) \left[\frac{\cos(\pi u)}{\prod_{l=0}^{N-1} \left(1 - \left(\frac{u}{\mu_l} \right)^2 \right)} \right] . \tag{26}$$

Note in the square brackets that at the poles, we have zero divided by zero. At a particular pole, we can evaluate the square bracket equation at some $u \to \mu_m$ by noting

$$F_a(\mu_m) = C\mu_m \left(\frac{\prod_{n=1}^{N-1} \left(1 - \left(\frac{\mu_m}{\sigma Z_n} \right)^2 \right)}{\prod_{\substack{l=0 \\ l \neq m}}^{N-1} \left(1 - \left(\frac{\mu_m}{\mu_l} \right)^2 \right)} \right) \lim_{u \to \mu_m} \left[\frac{\cos(\pi u)}{1 - \left(\frac{u}{\mu_m} \right)^2} \right] . \tag{27}$$

We evaluate this using L'Hôpital's rule, and arrive at the expression

$$F_a(\mu_m) = C\mu_m \left(\frac{\prod_{n=1}^{N-1} \left(1 - \left(\frac{\mu_m}{\sigma Z_n} \right)^2 \right)}{\prod_{\substack{l=0 \\ l \neq m}}^{N-1} \left(1 - \left(\frac{\mu_m}{\mu_l} \right)^2 \right)} \right) \left[\frac{\pi \mu_m \sin(\pi \mu_m)}{2} \right] , \tag{28}$$

which can be manipulated to

$$F_a\left(\mu_m\right)=\frac{C\,\pi\,{\mu_m}^2\sin\left(\pi\mu_m\right)}{2}\left(\frac{\prod_{n=1}^{N-1}\left(1-\left(\frac{\mu_m}{\sigma Z_n}\right)^2\right)}{\prod_{\substack{l=0\\ l\neq m}}^{N-1}\left(1-\left(\frac{\mu_m}{\mu_l}\right)^2\right)}\right). \tag{29}$$

Noting that $\mu_m = m+1/2$, this can be further simplified to

$$F_a\left(\mu_m\right)=\frac{C\,\pi\left(m+1/2\right)^2\left(-1\right)^m}{2}\left(\frac{\prod_{n=1}^{N-1}\left(1-\left(\frac{m+1/2}{\sigma Z_n}\right)^2\right)}{\prod_{\substack{l=0\\ l\neq m}}^{N-1}\left(1-\left(\frac{m+1/2}{\mu_l}\right)^2\right)}\right). \tag{30}$$

This expression is the asymptotic model for the difference function evaluated at the zero positions. The asymptotic model is an envelope for sidelobes.

The Result

The task now is to reconcile the IPR in Eq. (10) with the asymptotic model for the difference function in Eq. (30). Specifically, we will do so at the zeros $\mu_m = m + 1/2$.

Recall that the IPR is expressed as

$$F(u) = 2j \sum_{l=0}^{N-1} B_l \frac{(-1)^l u \cos(\pi u)}{(l+1/2)^2 - u^2} \ . \tag{31}$$

We evaluate this at $\mu_m = m + 1/2$ by the limit

$$F(\mu_m) = 2j \lim_{u \to \mu_m} \sum_{l=0}^{N-1} B_l \frac{(-1)^l u \cos(\pi u)}{(l+1/2)^2 - u^2} = j\pi B_m \ . \tag{32}$$

Specifically, we note that

$$F(\mu_m) = \lim_{u \to \mu_m} F(u) = j\pi B_m \ , \tag{33}$$

Which corrects a slight typographical error in Bayliss' equation Eq. (46).

We now equate this with Eq. (30) to yield

$$F(\mu_m) = F_a(\mu_m) \ . \tag{34}$$

This allows us to calculate the coefficients

$$B_m = \frac{1}{j\pi} F_a(\mu_m) \tag{35}$$

Combining this with Eq. (30) yields

$$B_m = \begin{cases} \dfrac{C}{2j}(m+1/2)^2 (-1)^m \left(\dfrac{\displaystyle\prod_{n=1}^{N-1} \left(1 - \left(\dfrac{m+1/2}{\sigma Z_n} \right)^2 \right)}{\displaystyle\prod_{\substack{l=0 \\ l \neq m}}^{N-1} \left(1 - \left(\dfrac{m+1/2}{l+1/2} \right)^2 \right)} \right) & m = 0, 1, 2, \cdots, N-1 \\ 0 & m = N, N+1, \cdots \end{cases} \tag{36}$$

This is Bayliss' Eq. (47) albeit with a slight correction of a typographical error. Nevertheless, this expression now gives the coefficients B_l in Eq. (7) to define the taper function.

We now offer some comments.

- As previously stated, Bayliss chose the constant C "so that the peak of the asymptotic difference pattern is unity." This implies that the asymptotic model for the difference function was real and odd. Since the IPR function $F(u)$ was chosen to match this, this also implies that the aperture illumination function was imaginary (in the complex sense) and odd. This is borne out by the coefficients B_m in Eq. (36) being imaginary as well.
- Traditionally, taper functions are taken to be real-valued. Since the taper function in this case is also odd, this implies that the IPR function $F(u)$ is imaginary and odd, common for phase-monopulse topologies. This further implies that we need to match it to an asymptotic model for the difference function $F_a(u)$ that is also imaginary. This can be accomplished by departing from Bayliss' choice and instead choosing C that is purely imaginary, perhaps with a peak value of $+j$. The coefficients B_m in Eq. (36) are thereby calculated to be real instead. With this small change, the derivation still remains valid.
- There is nothing magical about C being chosen to yield a peak of the asymptotic difference pattern with a unity magnitude, whether real or imaginary. Other magnitudes can work quite fine, too.
- We will henceforth refer to the angle $\theta = 0$ as the antenna "boresight" angle.

"It is remarkable how much long-term advantage people like us have gotten by trying to be consistently not stupid, instead of trying to be very intelligent."
-- Charlie Munger

3 Taper Design Procedure

Here we detail the procedure for designing a Bayliss taper suitable for programming a software function to do so.

Preliminary

Select the following input parameters.

S_{dB} = maximum sidelobe level with respect to difference pattern peak in dB,
N = approximate extent of equal sidelobe region, and
P = number of samples with which the Bayless window is divided. (37)

Step 1: Identify Secondary Constants

Initialize the following constants.

$T = 4$ = number of zeros to move, and
$C = 1$ = arbitrary temporary scaling constant. (38)

Step 2: Calculate Zero Positions

Calculate A, and zero positions $\xi_1, \xi_2, \xi_3, \xi_4$ using polynomial calculation of Eq. (17) and coefficients in Table 1.

Identify all zeros using Eq. (19).

Calculate dilation factor σ using Eq. (21).

Step 3: Calculate B Coefficients

Calculate B_m coefficients for $m = 0, \ldots, N-1$ using Eq. (36)

Step 4: Calculate Taper Function Samples

Divide the span $[-\pi, \pi]$ into P samples. An individual sample takes on a specific value x within this span.

Calculate taper function $g(x)$ using Eq. (7) along with Eq. (9).

Step 5: Correct Scaling of Taper Function

Convert to real-valued taper by multiplying by j, i.e., $g(x) \leftarrow jg(x)$.

Scale the taper to have unity peak value, i.e., $g(x) \leftarrow g(x) \Big/ \max\left(\left|g(x)\right|\right)$.

Note that the peak value for $\left|g(x)\right|$ may not always occur at one of the sampled values for x. Otherwise, other scaling criterial might also be used.

Gratuitous Comments

The procedure outlined above will yield the Bayliss taper, which is an aperture illumination function to yield a difference antenna pattern.

At times, it may be useful to employ a corresponding 'sum' antenna pattern for which we calculate a corresponding aperture illumination function as

$$g_s(x) = \left| g(x) \right|. \tag{39}$$

The sum and difference antenna patterns use aperture tapers that are thus interdependent.

Example

We illustrate the results of designing a Bayliss taper using the procedure above. Let us assume

$$\begin{aligned} &S_{dB} = -30 \text{ dB}, \\ &N = 10, \text{ and} \\ &P = 1000. \end{aligned} \tag{40}$$

Figure 2 illustrated the Bayliss taper and resulting IPR. Note that the near-in sidelobes are at the −30 dB design level, but begin falling off near the specified 10 nominal beamwidths from the center. Actually, the sidelobe at this position is −3 dB from the peak sidelobe level.

However, the corresponding sum pattern generated by the taper defined in Eq. (39) is displayed in Figure 3. We note that the well characterized sidelobes in the difference pattern come at the expense of rather horrible sidelobe response in the sum pattern. In this example, the first sidelobes are below the peak value by a mere 8.8 dB.

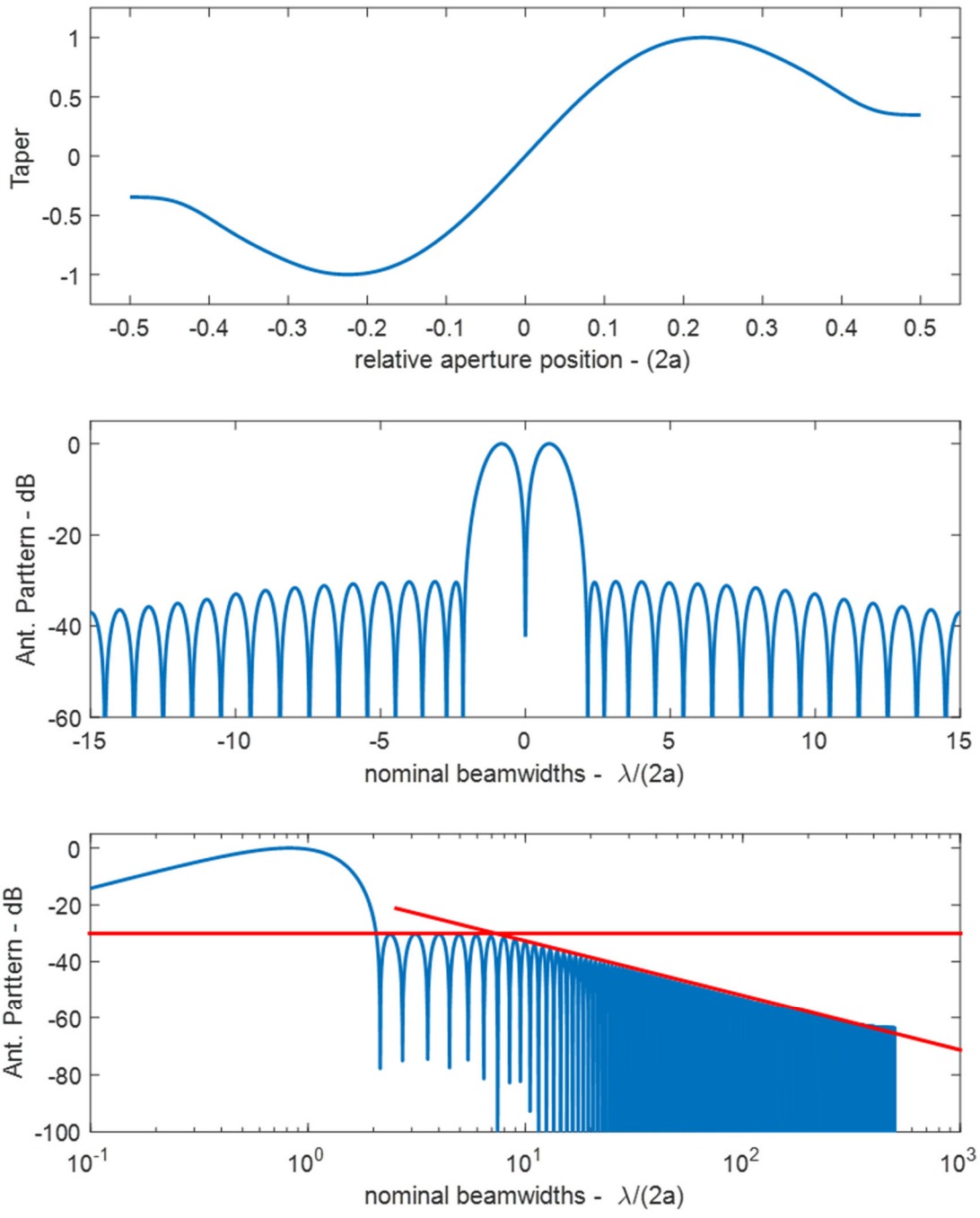

Figure 2. Bayliss taper designed for –30 dB sidelobes, and N=10, sampled for 1000 points.

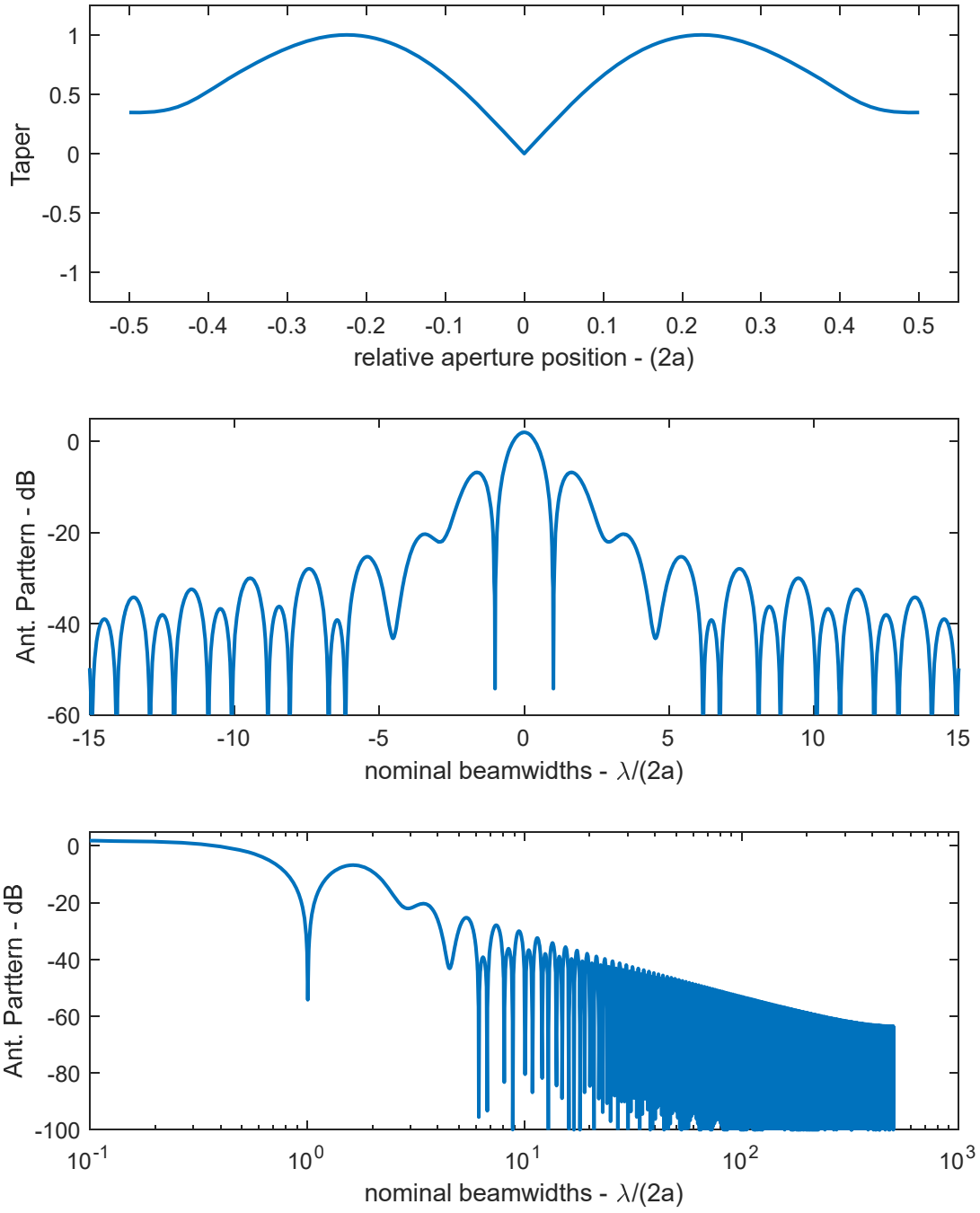

Figure 3. Sum taper and pattern created from Bayliss taper of Figure 2.

4 Monopulse Performance Parameters

The question now is "How well does the Bayliss taper perform?" Toward this end we examine several aspects of DOA performance.

The purpose of a monopulse antenna is to make accurate off-boresight DOA angle measurements. A reasonable question is "How well does the Bayliss taper facilitate this?" Toward answering this question, we examine several aspects of DOA performance with respect to the Bayliss taper.

We begin by recalling the description of the far-field antenna pattern of the Bayliss taper given in Eq. (31), also identified as the taper's IPR, with the specific coefficients defined by Eq. (36). We note that the far-field antenna pattern as a function of DOA angle requires combining Eq. (31) with Eq. (6).

We will generally follow the analysis methodology of an earlier report.[3] To facilitate clarity, it becomes convenient to divide the overall aperture into two halves, so that

$$\begin{aligned} -h_1(\theta) &= \text{beam pattern from left half of the aperture with a Bayliss taper, and} \\ h_2(\theta) &= \text{beam pattern from right half of the aperture with a Bayliss taper.} \end{aligned} \tag{41}$$

We will define sum and difference patterns as

$$\begin{aligned} d(\theta) &= \frac{h_2(\theta) - h_1(\theta)}{\sqrt{2}} = F(u)\Big|_{u=(2a/\lambda)\sin\theta} = \text{Bayliss taper IPR, and} \\ s(\theta) &= \frac{h_2(\theta) + h_1(\theta)}{\sqrt{2}} = \text{convenient sum pattern, derived from Eq. (39).} \end{aligned} \tag{42}$$

We here follow the convention of creating sum and difference signals in a manner to preserve power; hence the division by $\sqrt{2}$. Ultimately, however, this will not impact the performance results we seek. It just won't matter.

Let a target present received energy at some angle and amplitude, where

$$\begin{aligned} A_m &= \text{RX signal amplitude to the whole aperture, and} \\ \theta_m &= \text{DOA angle.} \end{aligned} \tag{43}$$

The precise value for signal amplitude A_m will as a practical matter, and thus necessarily, remain undefined. This is something we need to work around in the subsequent development.

The voltages generated for each half of the aperture are calculated to be

$$m_1 = \frac{A_m}{2} h_1(\theta_m) \quad \text{, and}$$
$$m_2 = \frac{A_m}{2} h_2(\theta_m) . \tag{44}$$

The voltages generated by the Bayliss taper pattern and the corresponding sum pattern are concocted to be

$$m_d = m_2 - m_1 = \frac{A_m}{\sqrt{2}} d(\theta_m) = \text{voltage generated by Bayliss taper pattern, and}$$
$$m_s = m_2 + m_1 = \frac{A_m}{\sqrt{2}} s(\theta_m) = \text{voltage generated by corresponding sum pattern.} \tag{45}$$

This of course implies that

$$d(\theta_m) = \left(\sqrt{2}/A_m\right) m_d \text{, and}$$
$$s(\theta_m) = \left(\sqrt{2}/A_m\right) m_s . \tag{46}$$

Our task is to estimate DOA angle θ_m from measurements m_d and m_s or equivalent, without specific knowledge of signal amplitude A_m.

4.1 Monopulse Slope

The monopulse slope, also called "difference slope," identifies the rate of change of the difference pattern response with respect to angle, normally evaluated at the center of the beam, in the boresight direction where $\theta = 0$. We begin with the first-order Taylor series expansion

$$d(\theta) \approx j k_d \theta = \text{difference signal approximation,} \tag{47}$$

where we identify the "monopulse slope" as

$$k_d = -j \frac{d}{d\theta} d(\theta)\Big|_{\theta=0} = -j\left(\frac{d}{du} F(u)\right)\left(\frac{d}{d\theta} u\right) = (4a/\lambda) \sum_{l=0}^{N-1} \frac{B_l (-1)^l}{(l+1/2)^2} . \tag{48}$$

For real coefficients B_l the monopulse slope is real-valued. We shall stipulate this going forward. This monopulse slope has units proportional to volts/angle. Furthermore, once a particular Bayliss taper is selected, then this is a constant.

It also follows from real coefficients B_l that $d(\theta)$ is imaginary, and $s(\theta)$ is real-valued. Using Eq. (47) we may calculate DOA for small angles as

$$\hat{\theta}_m = -j\frac{1}{k_d}d(\theta_m) = -j\frac{\sqrt{2}}{k_d A_m}m_d \text{ = DOA estimate.} \tag{49}$$

Note that m_d is a measurement, k_d is a known constant, but A_m is unknown, rendering it problematic to estimate $\hat{\theta}_m$ without employing more information. We will do so with $s(\theta_m)$ or equivalent.

4.2 Monopulse Ratio

We may normalize the difference pattern response by dividing by the sum pattern response, which is also proportional to A_m, thereby creating a monopulse ratio as

$$r(\theta_m) = \frac{m_d}{m_s} = \frac{d(\theta_m)}{s(\theta_m)} = \frac{j k_d \theta_m}{s(\theta_m)} \text{ = monopulse ratio.} \tag{50}$$

This ratio is solely a function of measurements. For small θ_m, we may assume a constant value for the sum pattern, and simplify

$$s(\theta_m) \approx s(0) = s_0 . \tag{51}$$

This is a known quantity as a function of the sum pattern taper.

Our DOA estimate can then be calculated as

$$\hat{\theta}_m = \frac{s_0}{k_d}\text{Im}\{r(\theta_m)\} . \tag{52}$$

The monopulse ratio embodies all the measurements, and the rest of the parameters on right side of the equation are known, or knowable, constants. Consequently, the DOA angle can now be estimated. We may manipulate Eq. (52) to a form

$$\hat{\theta}_m = \frac{\theta_{ref}}{k_m}\text{Im}\{r(\theta_m)\}, \tag{53}$$

where we define

$$k_m = \frac{k_d}{s_0}\theta_{ref} \text{ = normalized monopulse slope, with units V/V/beamwidth, and}$$

$$\theta_{ref} \text{ = nominal reference antenna pattern beamwidth.} \tag{54}$$

There is some latitude in defining the nominal reference antenna pattern beamwidth θ_{ref}. A particularly convenient reference beamwidth is

$$\theta_{ref} = \lambda/(2a). \tag{55}$$

This is the nominal beamwidth for a uniformly illuminated aperture, i.e., no taper at all, as for a line source with length $(2a)$ as defined in Eq. (1). This definition will allow a common reference for different tapers. However, whatever is chosen to calculate k_m in Eq. (54) should also be the same value as the overt parameter in the right side of Eq. (53). Noe that this reference pattern is generated from over the entire aperture, and not just from half of the aperture.

We do note that the IEEE defines the monopulse/difference slope as "the slope of the difference-pattern voltage (normalized with respect to the sum-pattern voltage) as a function of target angle from the tracking axis."[32] In spite of the IEEE definition, and to facilitate comparing monopulse performance parameters, we will assume a more generalized normalization of the monopulse slope against a common reference beamwidth such as Eq. (55), and a more general reference-pattern voltage, to be discussed next.

Generalizing the Sum Channel

We now revisit the assumption for the sum pattern in Eq. (42) and Eq. (45). These were derived assuming the sum pattern was calculated using the presumed taper of Eq. (39). We are now divorcing ourselves from this constraint.

We now allow ourselves to employ a second taper, requiring that it be real and even. We define this to be a reference taper, that is

$$g_{ref}(x) = \text{reference taper.} \tag{56}$$

This taper will produce a reference antenna pattern which we define as

$$s_{ref}(\theta) = \text{reference antenna pattern, corresponding to Eq. (56).} \tag{57}$$

Tapers of interest will produce a dominant mainlobe in the boresight direction at $\theta = 0$. The voltage generated by this antenna pattern becomes

$$m_{ref} = \frac{A_m}{\sqrt{2}} s_{ref}(\theta_m) = \text{voltage generated by corresponding reference pattern.} \tag{58}$$

Eq. (50) now becomes

$$r(\theta_m) = \frac{m_d}{m_{ref}} = \frac{d(\theta_m)}{s_{ref}(\theta_m)} = \frac{j k_d \theta_m}{s_{ref}(\theta_m)} = \text{monopulse ratio.} \tag{59}$$

We also now redefine

$$s_0 = s_{ref}\left(0\right). \tag{60}$$

With these new re-definitions, we may still calculate

$$\hat{\theta}_m = \frac{s_0}{k_d}\,\mathrm{Im}\left\{r\left(\theta_m\right)\right\} = \frac{\theta_{ref}}{k_m}\,\mathrm{Im}\left\{r\left(\theta_m\right)\right\}, \tag{61}$$

where now

$$k_m = \frac{k_d}{s_0}\theta_{ref}\,. \tag{62}$$

Nevertheless, we remain mindful that both $r\left(\theta_m\right)$ and k_m will depend on the specific reference antenna pattern $s_{ref}\left(\theta\right)$ used, and hence the specific reference taper $g_{ref}\left(x\right)$ from which it is calculated.

The bottom line is that using a reference antenna pattern $s_{ref}\left(\theta\right)$ is all about getting rid of A_m in Eq. (49), thereby eliminating the impact of target signal strength. The parameter s_0 is just a scale factor for A_m for small DOA angles with respect to the voltage measurement in Eq. (58). Any real and even taper pattern that generates a dominant mainlobe at $\theta = 0$ will do, as it will eventually divide out in Eq. (61). We just need to know what it is in the meantime.

4.3 DOA Angle Noise

We begin by expanding Eq. (61) using Eq. (59) to

$$\hat{\theta}_m = \frac{s_0}{k_d}\,\mathrm{Im}\left\{\frac{m_d}{m_{ref}}\right\}. \tag{63}$$

The error in this DOA angle estimate will depend primarily on the noise in the difference pattern measurement. That is, for signal measurement errors small with respect to m_{ref},

$$\varepsilon_{\hat{\theta}_m} \approx \frac{s_0}{k_d}\,\mathrm{Im}\left\{\frac{n_d}{m_{ref}}\right\} = \text{angle error in DOA estimate,} \tag{64}$$

where

n_d = complex noise in the difference pattern measurement, with zero mean, (65)

with variance

$$\sigma_d^2 = E\left\{\left|n_d\right|^2\right\} = \text{variance of } n_d . \tag{66}$$

The DOA angle estimate error can be expanded to

$$\varepsilon_{\hat{\theta}_m} \approx \frac{s_0}{k_d}\,\mathrm{Im}\left\{\frac{n_d}{\frac{A_m s_0}{\sqrt{2}}}\right\} = \text{angle in DOA estimate,} \tag{67}$$

The variances of the errors are related as

$$\sigma_{\hat{\theta}_m}^2 = E\left\{\left|\varepsilon_{\hat{\theta}_m}\right|^2\right\} \approx \left(\frac{s_0}{k_d \frac{A_m s_0}{\sqrt{2}}}\right)^2 \mathrm{Im}\left\{\sigma_d^2\right\} = \left(\frac{s_0}{k_d \frac{A_m s_0}{\sqrt{2}}}\right)^2 \frac{\sigma_d^2}{2} . \tag{68}$$

Note that the difference pattern measurement variance is divided by two because only the imaginary component is required. This may be rearranged to

$$\sigma_{\hat{\theta}_m}^2 \approx \left(\frac{s_0}{k_d}\right)^2 \frac{1}{2\left[\frac{A_m^2 s_0^2}{2\sigma_d^2}\right]} = \left(\frac{\theta_{ref}}{k_m}\right)^2 \frac{1}{2\left[\frac{A_m^2 s_0^2}{2\sigma_d^2}\right]} . \tag{69}$$

We identify the signal power generated by the reference pattern for a target in the boresight direction at $\theta_m = 0$ from Eq. (58) as

$$E\left\{\left|m_{ref}\right|^2\right\}\Big|_{\theta_m=0} = \frac{A_m^2 s_0^2}{2} . \tag{70}$$

Consequently, the quantity in the square brackets of Eq. (69) is a Signal-to-Noise Ratio (SNR). Specifically, this SNR is the ratio of the power in the reference pattern signal to the noise power in the difference pattern signal. That is.

$$SNR_{\Sigma/\Delta} = \left[\frac{A_m^2 s_0^2}{2\sigma_d^2}\right] = \text{reference pattern signal power to difference pattern noise power.} \tag{71}$$

Consequently, and customarily, Eq. (69) is usually expressed as

$$\sigma_{\hat{\theta}_m}^2 \approx \left(\frac{\theta_{ref}}{k_m} \right)^2 \frac{1}{2\,SNR_{\Sigma/\Delta}} \ , \tag{72}$$

or as is commonly expressed in terms of standard deviation

$$\sigma_{\hat{\theta}_m} \approx \frac{\theta_{ref}}{k_m \sqrt{2\,SNR_{\Sigma/\Delta}}} \ . \tag{73}$$

This is consistent with the result in an earlier report.[3]

We now offer some comments.

- SNR will most definitely depend on the specific aperture taper. This is explored in an earlier report.[5]
- Consider the case where Eq. (39) was true, that is, that the magnitudes of the sum and difference tapers were the same, only differing in phase for half the overall aperture. This is often a typical characteristic of most monopulse systems. In this case, the noise power in the sum channel measurement would be the same as the noise power in the difference channel measurement. That is, for this case

  $SNR_{\Sigma/\Delta} = SNR_{\Sigma}$ = SNR as measured in the sum channel only. (74)

- Now consider the case where Eq. (39) was not necessarily true, that is, the difference taper and the reference taper were not equal to each other in magnitude, resulting in unrelated antenna patterns. This will clearly impact s_0, and consequently also impact $SNR_{\Sigma/\Delta}$. However, it will also impact k_m, and do so in a manner that mitigates the impact of s_0 on the final DOA angle variance calculation. This is most obvious in the middle expression of Eq. (69), where we see s_0^2 in both numerator and denominator, with no other parameters dependent on s_0. This suggests that the reference taper, although impacting intermediate parameters, will ultimately not affect the noise in the DOA angle estimate. This is good to know.

  It would be negligent, however, to not share that the development in this section does depend on an underlying assumption that $SNR_{\Sigma/\Delta}$ is pretty good to begin with. This is essentially the condition imposed upon Eq. (64).

- We now address the question "If reference pattern doesn't matter, and difference pattern is zero in the boresight direction, then how can we really predict performance?"

  We answer this by noting that the basic equation for DOA angle noise variance is a simplification of Eq. (68), namely

$$\sigma_{\hat{\theta}_m}^2 = \left(\frac{1}{k_d \left(A_m / \sqrt{2} \right)} \right)^2 \frac{\sigma_d^2}{2} \ . \tag{75}$$

We observe again that a reference antenna pattern has no impact on this. Consequently, we may then choose 'any' convenient reference antenna pattern for an SNR calculation *specifically for the purpose of estimating DOA angle noise*. This reference pattern does not have to be the same as is later used in an operational implementation for actually estimating DOA angle. Accordingly, for this specific purpose only, we choose a reference antenna pattern derived from the aperture taper in Eq. (39). This then makes Eq. (74) true, and the DOA angle noise variance may be calculated as

$$\sigma_{\hat{\theta}_m}^2 \approx \left(\frac{s_0}{k_d} \right)^2 \frac{1}{2\,SNR_\Sigma} = \left(\frac{\theta_{ref}}{k_m} \right)^2 \frac{1}{2\,SNR_\Sigma} \ , \tag{76}$$

where we acknowledge that some of the other parameters in Eq. (76) now also depend on Eq. (39). We reiterate that this is true specifically for the case where Eq. (39) is true, repeated here as the sum pattern aperture taper

$$g_s(x) = \left| g(x) \right| . \tag{77}$$

When later a different reference antenna pattern is employed operationally, then parameters s_0, k_m, and $SNR_{\Sigma/\Delta}$ may change, but the DOA angle variance $\sigma_{\hat{\theta}_m}^2$ will remain the same, i.e., depending only on the unchanged parameters in Eq. (75).

4.4 Antenna Gain/Efficiency

The influence of antenna aperture tapers on TX and RX antenna gain, and performance efficiency with respect to uniform aperture illumination are discussed in an earlier report.[5]

5 Examples

We now provide some examples of Bayliss tapers with variations in various input parameters. Our baseline for comparison is the parameter set

$$\begin{aligned} &S_{dB} = -30 \text{ dB}, \\ &N = 10, \text{ and} \\ &P = 1000, \end{aligned} \tag{78}$$

which yielded the taper and antenna pattern in Figure 2. We repeat this case in Figure 4 with some additional information.

The sum pattern is that which is generated by Eq. (39).

The monopulse slope also assumes this sum pattern and a reference pattern beamwidth described by Eq. (55), numerically calculated from the monopulse ratio.

The pattern efficiency is the sum pattern gain with respect to that of a uniformly illuminated aperture.

Variations in Sidelobe Levels

Figure 5, Figure 6, and Figure 7 illustrate the impact of changing the sidelobe specification. We observe that as sidelobe specifications become increasingly lower, so too does the monopulse slope diminish, as well as the pattern efficiency diminishing.

Variations in Equal Sidelobe Span

Figure 8, Figure 9, and Figure 10 illustrate the effects of adjusting the span of equal sidelobes. We observe that as the equal sidelobe span increases, the monopulse slope also increases, and even the pattern efficiency also increases. Sidelobes falling off happens farther away from the center.

We also observe that in the taper itself, as the equal sidelobe span increases, spikes arise at the ends of the tapers, and become increasingly 'spikey' as the span increases further. These end spikes are sometimes called "inverse tapering," or "edge illumination."[‡‡]

This is also observed for the Taylor taper, especially as it approaches the Dolph-Chebyshev taper for equal sidelobe span. This is what makes the Dolph-Chebyshev taper impractical.

Variations in taper vector length

Figure 11 and Figure 12 illustrate the impact of the taper vector length on the pattern characteristics. Simply put, finer sampling of the taper yields higher fidelity results for the pattern.

[‡‡] To a lesser extent, these end spikes also begin to appear as sidelobe suppression becomes less severe.

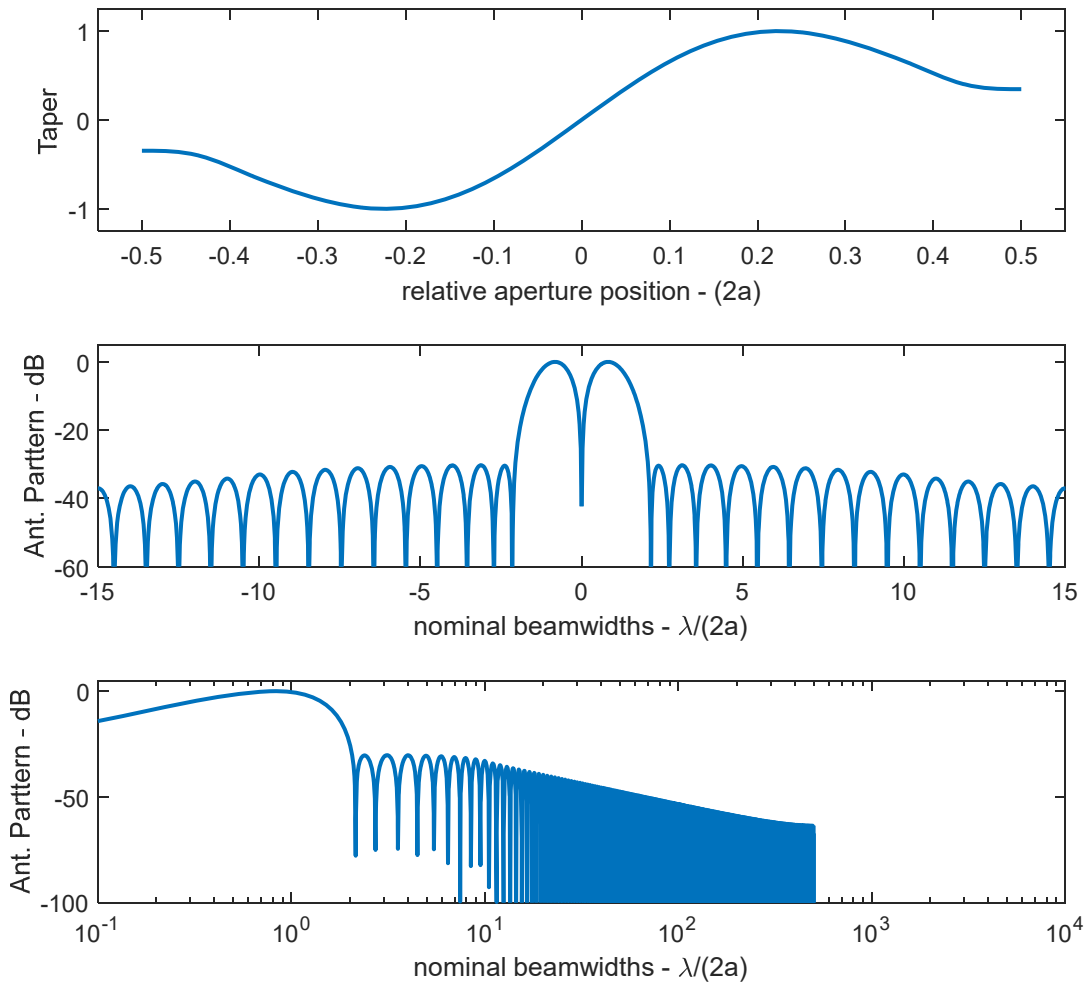

taper = Bayliss (sidelobes = -30 dB, N = 10)
sum pattern half-power beamwidth = 0.9255
monopulse slope = 0.9984*(π/2) at beam center
pattern efficiency = 0.8537 (-0.69 dB)

Figure 4. Baseline Bayliss taper for comparison.

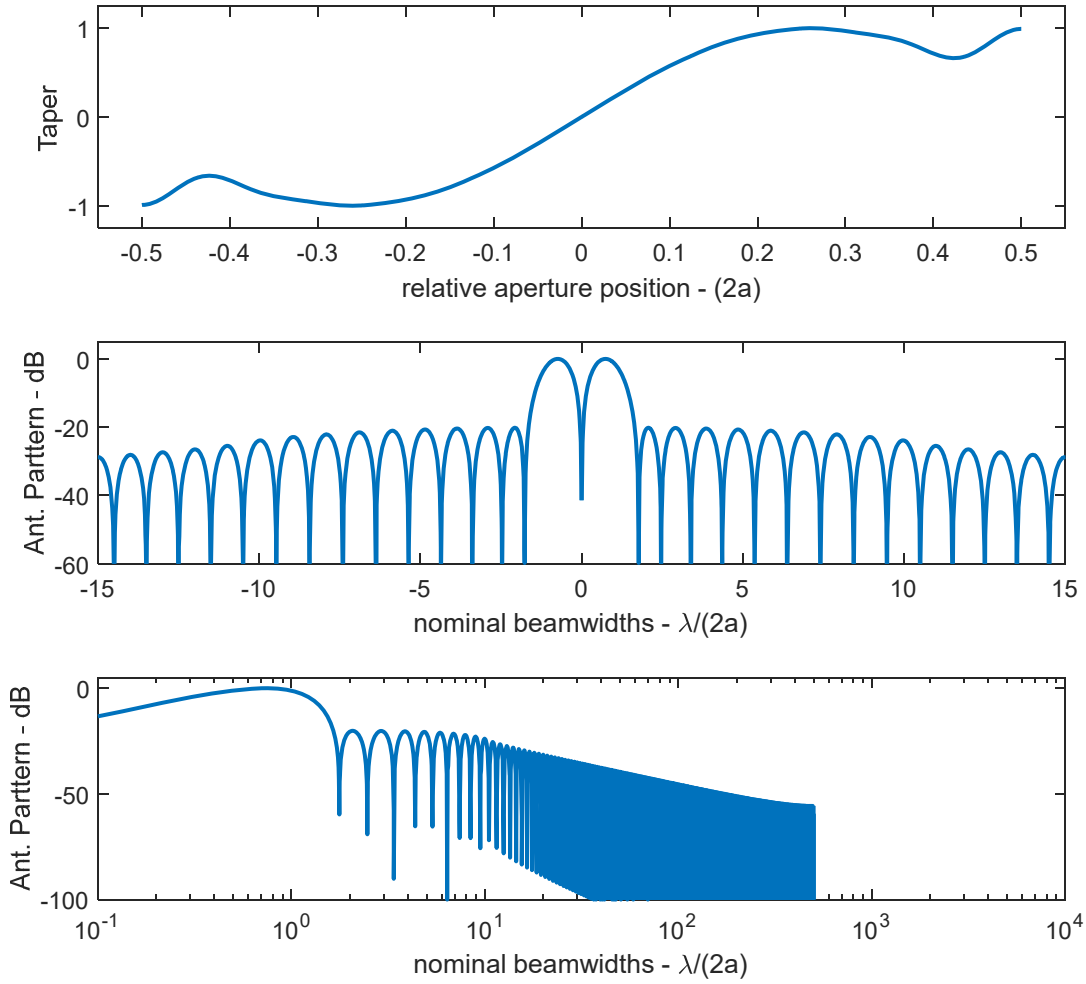

taper = Bayliss (sidelobes = -20 dB, N = 10)
sum pattern half-power beamwidth = 0.8248
monopulse slope = 1.1263*(π/2) at beam center
pattern efficiency = 0.8921 (-0.50 dB)

Figure 5. Bayliss taper for -20 dB sidelobes.

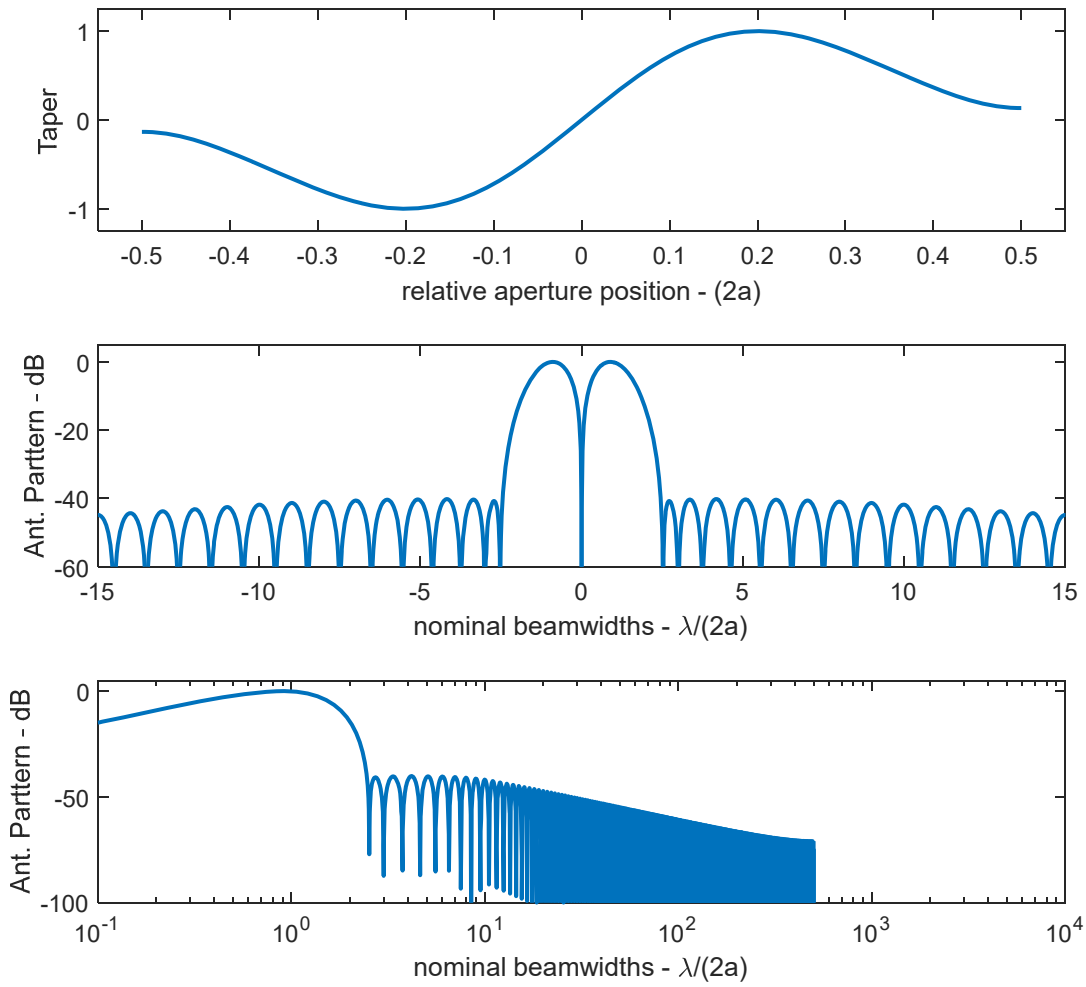

taper = Bayliss (sidelobes = -40 dB, N = 10)
sum pattern half-power beamwidth = 1.0099
monopulse slope = 0.9124*(π/2) at beam center
pattern efficiency = 0.7931 (-1.01 dB)

Figure 6. Bayliss taper for -40 dB sidelobes.

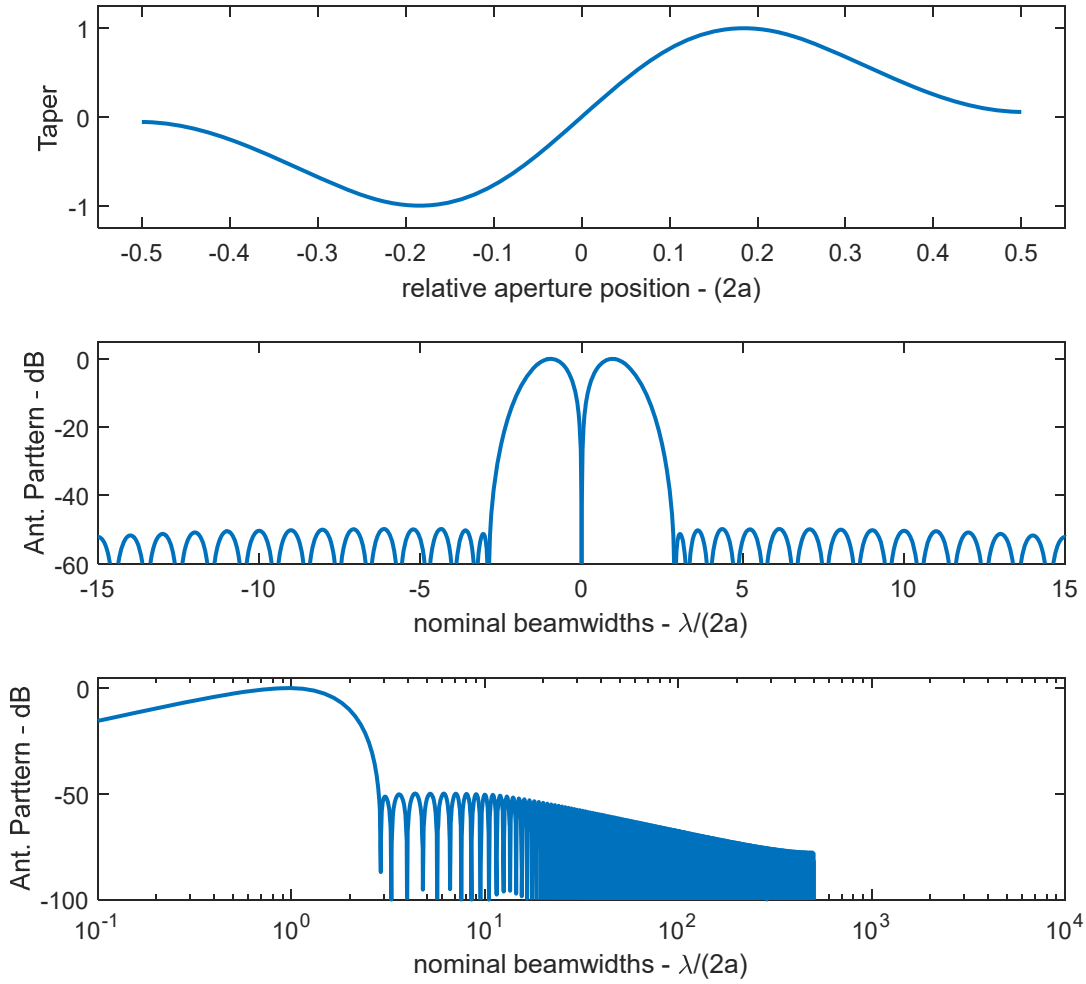

taper = Bayliss (sidelobes = -50 dB, N = 10)
sum pattern half-power beamwidth = 1.0823
monopulse slope = 0.8498*(π/2) at beam center
pattern efficiency = 0.7439 (-1.28 dB)

Figure 7. Bayliss taper for -50 dB sidelobes.

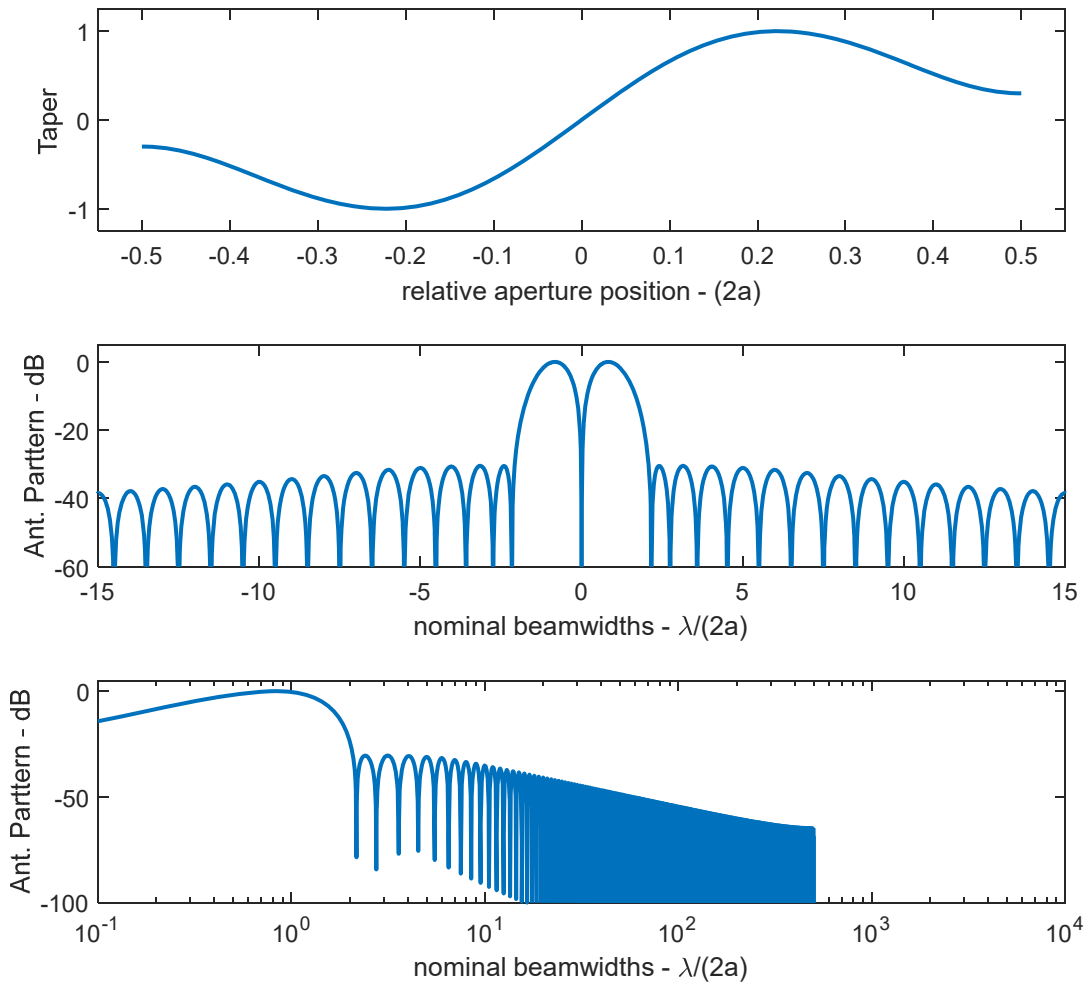

taper = Bayliss (sidelobes = -30 dB, N = 5)
sum pattern half-power beamwidth = 0.9324
monopulse slope = 0.9909*(π/2) at beam center
pattern efficiency = 0.8486 (-0.71 dB)

Figure 8. Bayliss taper for $N = 5$.

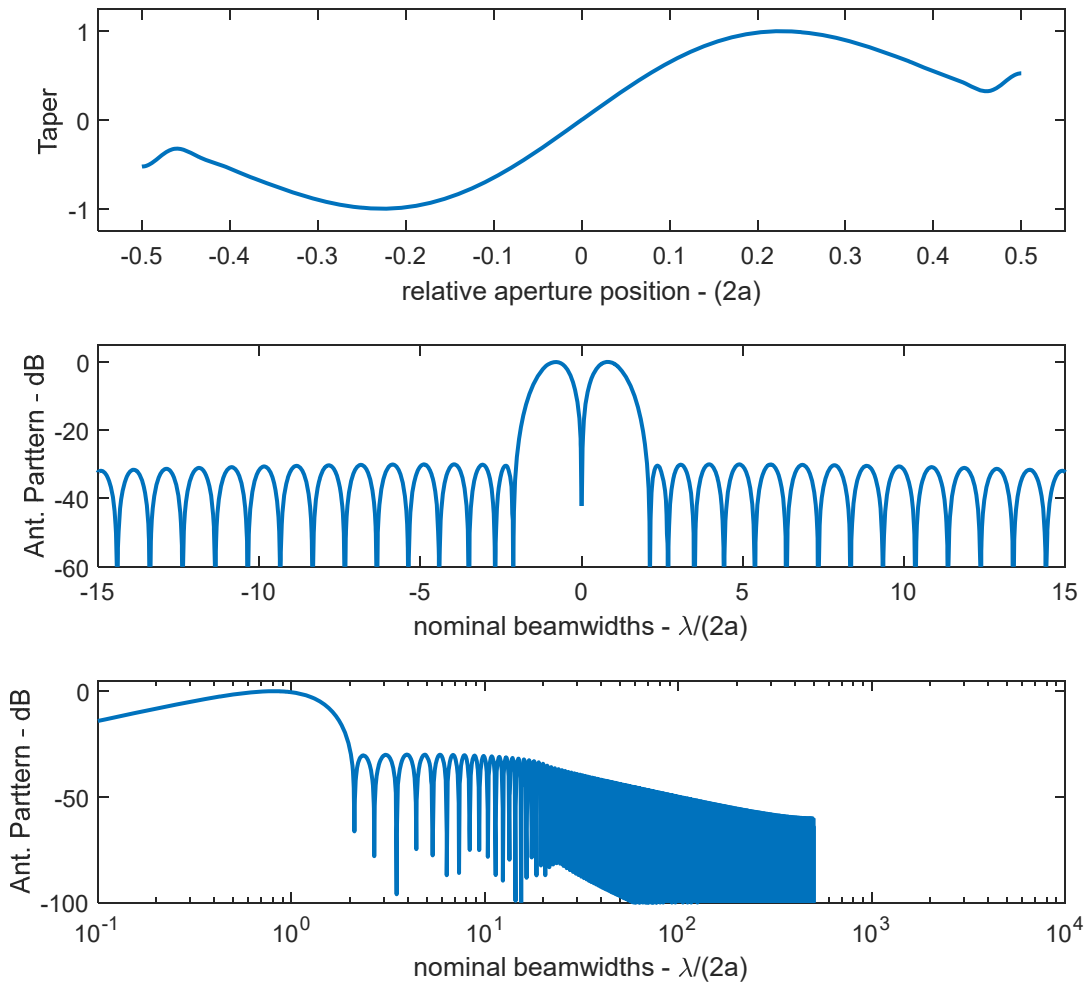

taper = Bayliss (sidelobes = -30 dB, N = 20)
sum pattern half-power beamwidth = 0.9133
monopulse slope = 1.0118*(π/2) at beam center
pattern efficiency = 0.8609 (-0.65 dB)

Figure 9. Bayliss taper for $N = 20$.

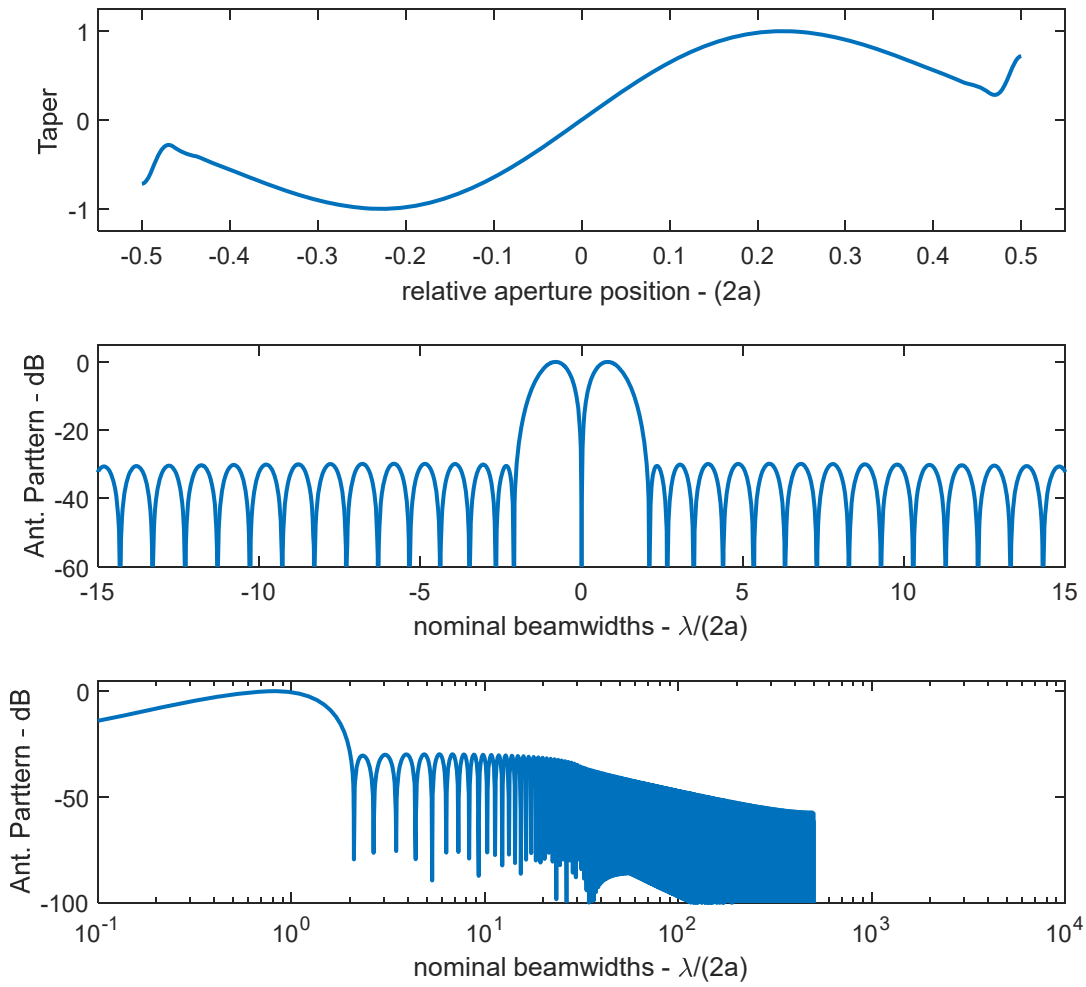

taper = Bayliss (sidelobes = -30 dB, N = 30)
sum pattern half-power beamwidth = 0.9075
monopulse slope = 1.0182*(π/2) at beam center
pattern efficiency = 0.8620 (-0.65 dB)

Figure 10. Bayliss taper for $N = 30$.

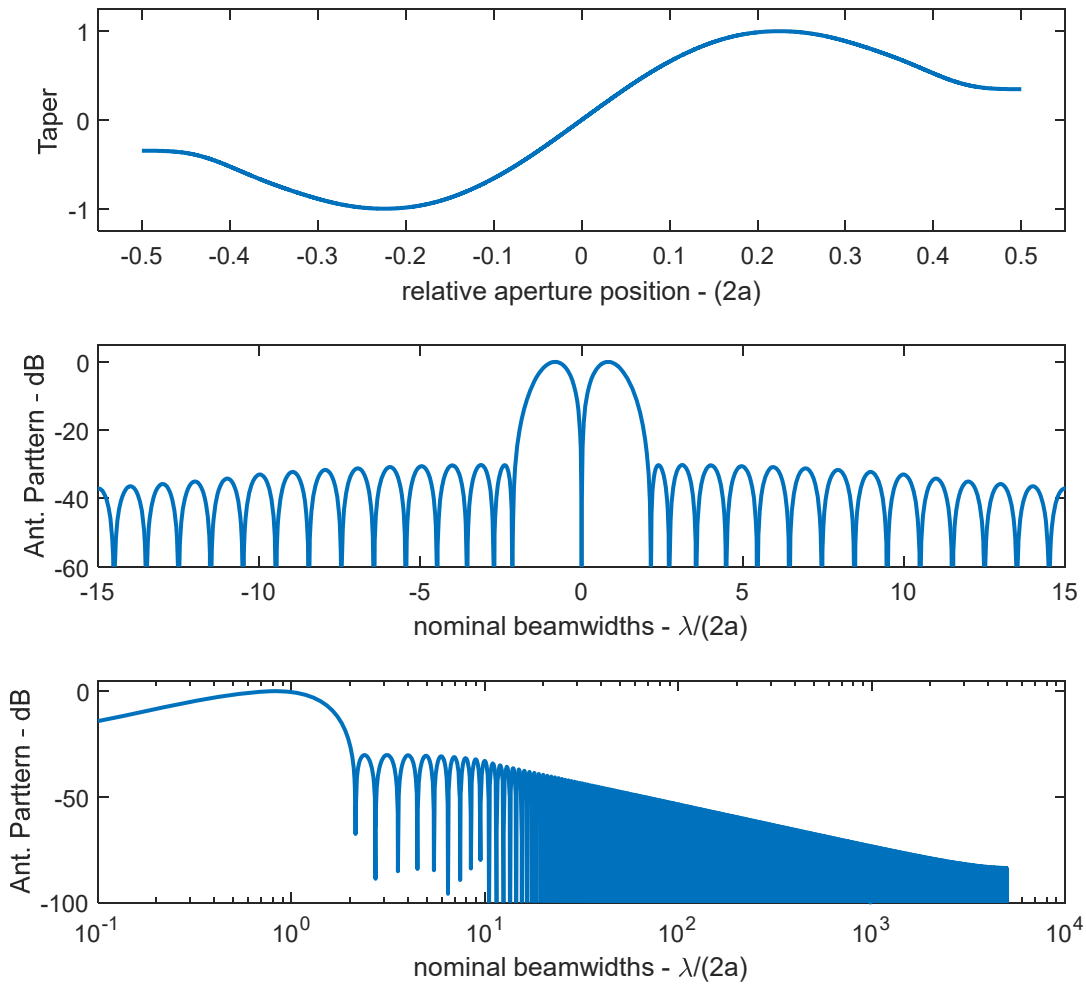

taper = Bayliss (sidelobes = -30 dB, N = 10)
sum pattern half-power beamwidth = 0.9251
monopulse slope = 0.9989*(π/2) at beam center
pattern efficiency = 0.8538 (-0.69 dB)

Figure 11. Bayliss taper with 10,000 samples.

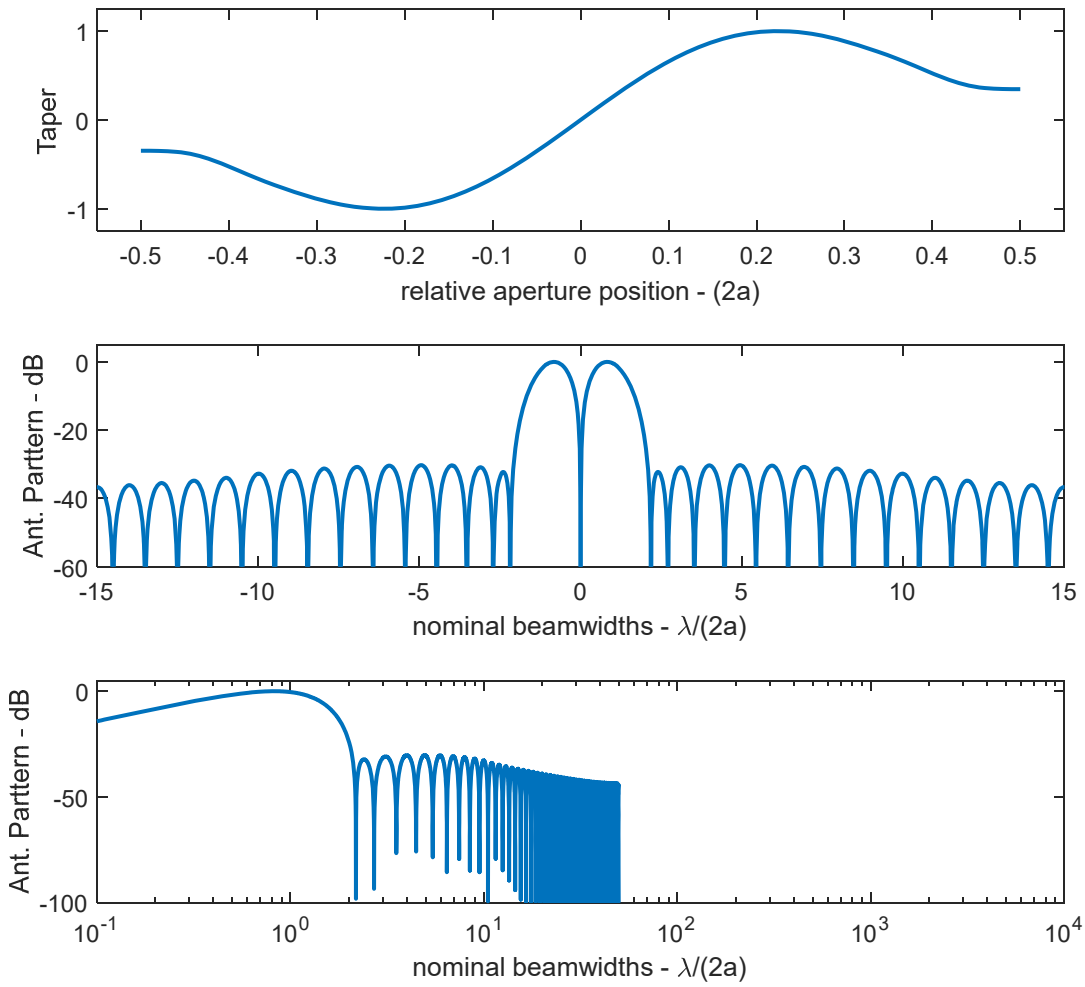

taper = Bayliss (sidelobes = -30 dB, N = 10)
sum pattern half-power beamwidth = 0.9290
monopulse slope = 0.9941*(π/2) at beam center
pattern efficiency = 0.8524 (-0.69 dB)

Figure 12. Bayliss taper with 100 samples.

6 Implementation Issues

In a perfect world we would get we whatever we want, or at least these authors would. Alas, practical implementation issues will limit or at least influence our choices with respect to antenna pattern generation, and ultimate performance. We explore several aspects of this below. We will presume a monostatic radar antenna arrangement.

Ultimately, we wish to identify when and how it makes sense to use a Bayliss taper.

6.1.1 Two-Way Antenna Patterns

Confining ourselves to a single antenna dimension, we observe that there are three distinct antenna patterns with which we concern ourselves.

1. TX pattern
2. RX sum/reference pattern
3. RX difference pattern

These patterns may all be independent of each other, or may exhibit some interdependencies. By extension, so too for the tapers that generate the antenna patterns.

Nevertheless, radar echo signals received by the RX sum channel will exhibit characteristics of the product of the TX pattern and the RX sum/reference pattern.

Similarly, radar echo signals received by the RX difference channel will exhibit characteristics of the product of the TX pattern and the RX difference pattern.

These combination patterns are called "two-way" antenna patterns. Of course, additive interference signals will not depend on the TX antenna. Nevertheless, since radar echo signals embody the two-way patterns, the specific contributions of TX versus RX patterns are indistinguishable in the radar echo return signals. Consequently, the burden of providing low antenna pattern sidelobes does not necessarily need to rest on the RX antennas alone. The TX antenna pattern can provide a substantial amount of this. This becomes a system design choice.

We do note that often the desire to transmit maximum power will typically need the TX aperture taper to be uniform.[5] We acknowledge that there may be other reasons for specific TX aperture tapers that constrain our choices in this regard.

Nevertheless, for the following discussion we will assume that our principal mechanism for controlling the two-way patterns is via the RX antenna patterns.

6.1.2 Sidelobe Requirements

Choosing a particular aperture taper is mainly about antenna pattern sidelobes. Requirements for how much sidelobe suppression is necessary in the RX antenna patterns is very radar application or mode dependent, as well as dependent on how much suppression is already provided by the TX antenna pattern. For example, a ground-based tracking radar might have very different needs than an airborne Intelligence, Surveillance, and Reconnaissance (ISR) radar. Exploring the universe of radar applications for sidelobe requirements is beyond the scope of this report. Nevertheless, we will offer a handful of very general observations.

RX Sum/Reference Antenna Pattern

The RX sum/reference channel isolates a target DOA to within the antenna beam, intended to be the mainlobe of the antenna beam. Undesired radar echo signals, characterized as "clutter," entering via RX antenna pattern sidelobes may be falsely detected and/or have their DOA mischaracterized, so this is undesirable.

Furthermore, for moving radar systems (e.g., airborne ISR radar), DOA is also often associated with Doppler due to radar velocity, as for Synthetic Aperture Radar (SAR). In Ground Moving Target Indicator (GMTI) radar systems, stationary ground clutter is limited to a presumed well-defined band of Doppler frequencies defined by the antenna mainlobe response, often called a "clutter band" or "clutter ridge" in range-Doppler maps. Radar signals falling outside of this clutter band are presumed to be moving targets. Consequently, unanticipated clutter echo energy allowed by excessive sidelobes can be falsely detected as moving targets, or even mask otherwise legitimate moving targets.[33] In pulse-Doppler radar systems, sidelobe clutter might even be aliased to other DOA angles, even those within the antenna pattern mainlobe. We don't like this.

Typical sidelobe suppression level requirements will depend on allowable false alarm statistics as well as the specific target Radar Cross Section (RCS) that we wish to detect.[34,35] Overall sidelobe suppression levels greater than 55 dB can easily be justified.

In any case, we desire RX sum/reference pattern sidelobes to be suppressed to levels that would generally avoid targets at erroneous DOA angles from being detected or otherwise interfering with legitimate detections.

We do note that should sidelobes not be adequately suppressed, then it might be possible to employ a "guard" channel to identify sidelobe responses, thereby allowing such signals to be ignored or perhaps even compensated.

RX Difference Antenna Pattern

Difference patterns are used to make fine DOA measurements near the boresight $\theta = 0$ direction of the antenna. Angle measurements are necessarily confined to the central monotonic and nearly linear slope region of the difference pattern.

For tracking radars, the difference pattern response provides an error signal to facilitate steering the antenna beam and keeping an antenna "locked" onto a specific target.

As with the sum/reference beam, for moving radar systems (e.g., airborne ISR radar), the DOA measure provided by the difference beam allows for discrimination of moving targets with respect to stationary clutter. Also, as with sum/reference beams, in pulse-Doppler radar systems, difference beam sidelobe clutter might be aliased to Doppler regions associated with other DOA angles, thereby perturbing measurements and interfering with clutter cancellation and moving target detection generally. We don't like this, either.

Bottom Line

So, ideally, we basically want low sidelobes in both the RX sum/reference antenna beam pattern, as well as the RX difference antenna beam pattern, that is, if we can get it.

6.1.3 Independent Sum and Difference Tapers

Ideally, we wish to implement independent sum/reference and difference antenna patterns simultaneously. For example, we might simultaneously implement a Bayliss difference antenna pattern and perhaps a Taylor reference antenna pattern, and optimize each independently. This was, in fact, a presumption by Bayliss in his paper. This would generally require simultaneous application of different aperture taper functions, which can be problematic, but not impossible. Among several techniques for doing so are the following.

1. We might employ dual analog beamformers behind an array antenna, with each beamformer allowing for different aperture tapering weights. This is doable, but a certainly a complication to overall system design.
2. We might employ digital beamforming, where individual elements have their RX signals digitized, and beamforming occurs via Digital Signal Processing (DSP) on essentially sampled and recorded contemporaneous data. In this manner, the digitized data can be reused with any number of taper functions, with multiple antenna beam patterns formable at our leisure.
3. If we are limited to but a single taper at any one time, but the taper is easily programmable, then we could consider interleaving reference and Bayliss tapers from pulse to pulse in a pulse-Doppler radar. This cuts the effective Pulse Repetition Frequency (PRF) in half, and may require some data corrections due to the slight timing offsets for the reference and difference pattern data.

6.1.4 Interdependent Tapers

In many radar systems we are limited with the tapers available to us. Here we address the conventional case where Eq. (39) is true, that is, say, specifically sum tapers and difference tapers have the same magnitude, and differ only in that half the difference aperture is given a π phase shift with respect to the same portion of the sum taper.

Our choice for contemporaneous RX sum and RX difference patterns boils down to trading sidelobe performance between these patterns. A pattern from a Taylor sum taper will give us high sidelobes in the difference antenna pattern. Similarly, a pattern from a Bayliss difference taper will give us high sidelobes in the sum antenna pattern. This becomes a "pick your poison" exercise.

A remaining option is to employ a taper in the TX aperture to mitigate two-way antenna pattern sidelobes for all RX channels. This, of course, has its own drawbacks.[5] In addition, as previously mentioned, high sum-pattern sidelobes can somewhat be addressed with a guard channel.

Finding some happy medium between sidelobe performance for codependent sum and difference tapers is beyond the scope of this report. We opine that the prospect for achieving satisfactory overall performance seems challenging. Nevertheless, the possibility exists for some circumstances.

7 Comments and Conclusions

Some observations are worth repeating here.

- The Bayliss taper effectively lowers difference pattern sidelobes, as it was designed to do. Sidelobe levels and other characteristics are essentially programmable.
- A sum pattern generated from the Bayliss taper, with magnitude taper values equal to the magnitude of the Bayliss taper, differing only in phase for half the aperture, will exhibit problematic high sidelobes.
- The Bayliss taper is most effective when used with a separate independent reference pattern taper, but then requires multiple beamformers for the same aperture. This is a complication that must be addressed.
- A straightforward Bayliss taper design procedure was presented.

Figure 13. "Rainbow" (courtesy Miss Sloane Doerry, age 3)

"The way I see it, if you want the rainbow, you got to put up with the rain."
-- Dolly Parton

References

[1] Edward T. Bayliss, "Design of monopulse antenna difference patterns with low sidelobes," *Bell System Technical Journal*, Vol. 47, No. 5, pp. 623-650, May 1968.

[2] Samuel M. Sherman, David K. Barton, *Monopulse Principles and Techniques – second edition*, ISBN-13: 978-1580531689, Artech House, Inc., 2011.

[3] Armin W. Doerry, Douglas L. Bickel, *Notes on Amplitude versus Phase Comparison Monopulse Antennas for Radar*, Sandia National Laboratories Report SAND2024-06153, Unlimited Release, May 2024.

[4] Armin W. Doerry, *Catalog of Window Taper Functions for Sidelobe Control*, Sandia National Laboratories Report SAND2017-4042, Unlimited Release, April 2017.

[5] Armin W. Doerry, *Notes on Tapered Active Array Antenna Performance*, Sandia National Laboratories Report SAND 2025-02426, Unlimited Release, February 2025.

[6] Robert J. Mailloux, *Phased Array Antenna Handbook, Third Edition*, ISBN-13: 978-1-63081-029-0, Artech House, Inc., 2018.

[7] Robert S. Elliott, *Antenna Theory & Design*, ISBN: 9780471449966, Wiley-IEEE Press, 2003.

[8] J. P. Shelton, *Synthesis of Taylor and Bayliss Patterns for Linear Antenna Arrays*, Naval Research Laboratory Report 8511, approved for public release, distribution unlimited, August 31, 1981.

[9] Srinivasa Rao Zinka, Jeong Phill Kim, "On the Generalization of Taylor and Bayliss n-bar Array Distributions," *IEEE Transactions on Antennas and Propagation*, Vol. 60, No. 2, pp. 1152-1157, February 2012.

[10] M. Alvarez-Folgueiras, J. A. Rodriguez-Gonzalez, F. Ares-Pena, "Sum and Difference Pattern with Common Aperture Tail," *Proceedings of the 2009 IEEE Antennas and Propagation Society International Symposium*, pp. 1-4, June 1, 2009.

[11] F. Ares, S. R. Rengarajan, J. A. Rodriguez, E. Moreno, "Optimal Compromise Among Sum and Difference Patterns Through Sub-Arraying," *Proceedings of the IEEE Antennas and Propagation Society International Symposium*, Vol. 2, pp. 1142-1145, July 21, 1996.

[12] David K. Barton, "History of Monopulse Radar in the US," *IEEE Aerospace and Electronic Systems Magazine*, Vol. 25, No. 3, pp. c1-c16, March 2010.

[13] Hu Hang, Diao Hongcui, Xv Ying, "Monopulse characteristic Based on Full Digital Weighting for Phased Array Radar at Subarray Level," *Proceedings of the 3rd IEEE International Symposium on Microwave, Antenna, Propagation and EMC Technologies for Wireless Communications*, pp. 693-696, October 27, 2009.

[14] Richard Kinsey, "Monopulse Stick Phased Array," *Proceedings of the 1995 Antenna Applications Symposium*, Vol. 20, pp. 138-167, May 1996.

[15] Robert S. Elliott, "Design of Line Source Antennas for Difference Patterns with Sidelobes of Individually Arbitrary Heights," *IEEE Transactions on Antennas and Propagation*, Vol. AP-24, No. 3, pp. 310-316, May 1976.

[16] D. A. McNamara, *On the Synthesis of Optimum Monopulse Antenna Array Distributions*, Ph.D. Thesis, University of Cape Town, September 1986.

[17] E. Botha, D. A. McNamara, "Direct Synthesis of Near-Optimum Difference Patterns for Planar Arrays," *Electronics Letters*, Vol. 28, No. 8, pp. 753-675, April 9, 1992.

[18] D. A. McNamara, "Optimum Monopulse Linear Array Excitations Using Zolotarev Polynomials," *Electronics Letters*, Vol. 21, No. 16, pp. 681-682, 1 August 1985.

[19] D. A. McNamara, "Direct synthesis of optimum difference patterns for discrete linear arrays using Zolotarev distributions," *IEE Proceedings-H*, Vol. 140, No. 6, pp. 495-500, December 1993.

[20] D. A. McNamara, "Performance of Zolotarev and modified-Zolotarev difference pattern array distributions," *IEE Proceedings Microwaves Antennas Propagation*, Vol. 141, No. 1, pp. 37-44, February I994.

[21] Miroslav Vlcek, Rolf Unbehauen, "Zolotarev Polynomials and Optimal FIR Filters," *IEEE Transactions on Signal Processing*, Vol. 47, No. 3, pp. 717-730, March 1999.

[22] Ralph Levy, "Generalized Rational Function Approximation in Finite Intervals Using Zolotarev Functions," *IEEE Transactions on Microwave Theory and Techniques*, Vol. Mtt-18, No. 12, pp. 1052-1064, December 1970.

[23] Siddharth Pal, Aniruddha Basak, Swagatam Das, P.N. Suganthan, "Synthesis of Difference Patterns for Monopulse Antenna Arrays – An Evolutionary Multi-objective Optimization Approach," *Proceedings of the 8th International Conference on Simulated Evolution and Learning (SEAL 2010)*, pp. 504-513, Kanpur, India, December 1-4, 2010.

[24] P. López, J. A. Rodríguez, F. Ares, E. Moreno, "Subarray Weighting for the Difference Patterns of Monopulse Antennas: Joint Optimization of Subarray Configurations and Weights," *IEEE Transactions on Antennas and Propagation*, Vol. 49, No. 11, pp. 1606-1608, November 2001.

[25] Peter W. Hannan, Patricia A. Loth, "A Monopulse Antenna Having Independent Optimization of The Sum and Difference Modes," 1958 IRE International Convention Record, Vol. 9, pp. 57-60, 21 March 1966.

[26] Peter W. Hannan, "Maximum Gain in Monopulse Difference Mode," *IRE Transactions on Antennas and Propagation*, Vol. 9, No. 3, pp. 314-315, May 1961.

[27] Peter W. Hannan, "Optimum Feeds for All Three Modes of a Monopulse Antenna I: Theory," *IRE Transactions on Antennas and Propagation*, Vol. 9, No. 5, pp. 444-454, September 1961.

[28] Peter W. Hannan, "Optimum Feeds for All Three Modes of a Monopulse Antenna I: Practice," *IRE Transactions on Antennas and Propagation*, Vol. 9, No. 5, pp. 454-461, September 1961.

[29] Thomas Tallott Taylor, "Design of line-source antennas for narrow beamwidth and low side lobes," *Transactions of the IRE Professional Group on Antennas and Propagation*, Vol. 3, No. 1, pp. 16-28, Jan. 1955.

[30] Thomas Tallott Taylor, "Design of circular apertures for narrow beamwidth and low sidelobes," *IRE Transactions on Antennas and Propagation*, Vol. 8, No. 1, pp. 17-22, January 1960.

[31] Charles L. Dolph, "A Current Distribution for Broadside Arrays Which Optimizes the Relationship between Beam Width and Side-Lobe Level," *Proceedings of the IRE*, Vol. 34, No. 6, pp. 335-348, June 1946.

[32] *IEEE Standard Radar Definitions*, IEEE Aerospace and Electronic Systems Society, Sponsored by the Radar Systems Panel, IEEE Std 686-2008, 21 May 2008.

[33] Armin W Doerry, Douglas L Bickel, *Antenna Requirements for GMTI Radar Systems*, Sandia National Laboratories Report SAND2020-2378, Unlimited Release, February 2020.

[34] Ann Marie Raynal, Bryan L. Burns, Tobias J. Verge, Douglas L. Bickel, Ralf Dunkel, Armin W. Doerry, "Radar cross section statistics of dismounts at Ku-band," SPIE 2011 Defense & Security Symposium, *Radar Sensor Technology XV*, Vol. 8021, Orlando FL, 25-29 April 2011.

[35] Ann Marie Raynal, Douglas L. Bickel, Michael M. Denton, Wallace J. Bow, Armin W. Doerry, "Radar cross section statistics of ground vehicles at Ku-band,"SPIE 2011 Defense & Security Symposium, *Radar Sensor Technology XV*, Vol. 8021, Orlando FL, 25-29 April 2011.

“I don't care about what anything was DESIGNED to do, I care about what it CAN do.”
-- Gene Kranz, NASA Flight Director, played by Ed Harris in “Apollo 13,”
produced by Imagine Entertainment, distributed by Universal Pictures, 1995.

Distribution

Unlimited Release

Email—Internal

all members	0534x	
Technical Library	01911	sanddocs@sandia.gov

Sandia National Laboratories is a multimission laboratory managed and operated by National Technology & Engineering Solutions of Sandia LLC, a wholly owned subsidiary of Honeywell International Inc. for the U.S. Department of Energy's National Nuclear Security Administration under contract DE-NA0003525.